

Vector Copula Variational Inference and Dependent Block Posterior Approximations

Yu Fu, Michael Stanley Smith and Anastasios Panagiotelis

March 4, 2025

Yu Fu is a PhD student and Michael Smith is Chair of Management (Econometrics), both at the Melbourne Business School, University of Melbourne, Australia. Anastasios Panagiotelis is Associate Professor of Business Analytics at University of Sydney, Australia. Correspondence should be directed to Michael Smith at mikes70au@gmail.com.

Acknowledgments: Yu Fu gratefully acknowledges support from the University of Melbourne through the Faculty of Business and Economics Graduate Research Scholarship and Henry Buck Scholarship. Michael Smith's research is supported by Australian Research Council Discovery Project DP250101069. We thank Jordan G. Bryan, David Nott and Lin Deng for helpful comments.

Vector Copula Variational Inference and Dependent Block Posterior Approximations

Abstract

Variational inference (VI) is a popular method to estimate statistical and econometric models. The key to VI is the selection of a tractable density to approximate the Bayesian posterior. For large and complex models a common choice is to assume independence between multivariate blocks in a partition of the parameter space. While this simplifies the problem it can reduce accuracy. This paper proposes using vector copulas to capture dependence between the blocks parsimoniously. Tailored multivariate marginals are constructed using learnable cyclically monotone transformations. We call the resulting joint distribution a “dependent block posterior” approximation. Vector copula models are suggested that make tractable and flexible variational approximations. They allow for differing marginals, numbers of blocks, block sizes and forms of between block dependence. They also allow for solution of the variational optimization using fast and efficient stochastic gradient methods. The efficacy and versatility of the approach is demonstrated using four different statistical models and 16 datasets which have posteriors that are challenging to approximate. In all cases, our method produces more accurate posterior approximations than benchmark VI methods that either assume block independence or factor-based dependence, at limited additional computational cost.

Keywords: Cyclically monotone transformation; Re-parameterization trick; Shrinkage priors; Variational Bayes; Vector copula

1 Introduction

Variational inference (VI) methods are a scalable alternative to Markov chain Monte Carlo (MCMC) methods for computing Bayesian inference; for some recent applications in econometric modeling, see [Koop and Korobilis \(2023\)](#), [Loaiza-Maya and Nibbering \(2023\)](#), [Bernardi et al. \(2024\)](#) and [Deng et al. \(2024\)](#). VI methods minimize the divergence between the posterior density and an approximating density $q \in \mathcal{Q}$. Key to the success of VI is the selection of a distributional family \mathcal{Q} that balances approximation accuracy with the speed at which this optimization problem can be solved. For the large and complex models for which VI is favored, one popular approach is to partition the model parameters into blocks that are assumed independent, but with multivariate marginals that are tailored to the statistical model. This is called a mean field or factorized approximation ([Ormerod and Wand, 2010](#)). Large and complex models where such approximations have been used to compute VI include random effects models ([Goplerud, 2022](#), [Menictas et al., 2023](#)), vector autoregressions ([Bernardi et al., 2024](#)), state space models ([Quiroz et al., 2023](#)), tobit models ([Danaher et al., 2020](#)), and topic models ([Ansari et al., 2018](#)) among others. However, the impact on posterior approximation accuracy of this independence assumption is rarely studied. In this paper, we use the recent idea of a vector copula ([Fan and Henry, 2023](#)) to capture dependence between the blocks parsimoniously, while retaining tailored multivariate marginals. We show how this can improve approximation accuracy with limited increase in the computation time. We refer to the approximation as a “dependent block posterior” and call our new method “vector copula variational inference” (VCVI).

Conventional copula models ([Nelsen, 2006](#)) couple (strictly) univariate marginals together to create a dependent joint distribution, and have been used previously as variational approximations ([Tran et al., 2015](#), [Han et al., 2016](#), [Gunawan et al., 2024](#)). In particular, implicit copula models that are constructed through element-wise transformation of the model parameters—which include elliptical and skew-elliptical copulas—make highly scalable approximations ([Smith et al., 2020](#), [Smith and Loaiza-Maya, 2023](#), [Salomone et al., 2023](#)). They are also fast to calibrate be-

cause they allow easy application of the re-parameterization trick (Kingma and Welling, 2013) in stochastic gradient descent (SGD) algorithms, to provide efficient solution of the variational optimization (Salimans and Knowles, 2013, Titsias and Lázaro-Gredilla, 2014).

Conventional copula models are based on Sklar’s theorem, which unfortunately cannot be employed with multivariate marginals (Genest et al., 1995). However, Fan and Henry (2023) suggest an extension that they call “Vector Sklar’s Theorem”, where each block of a random vector is transformed to a multivariate uniform distribution by a cyclically monotone function. A vector copula is then a distribution function on the product space of these multivariate uniform distributions. Fan and Henry (2023) show that the density of a multivariate distribution can be expressed analytically in terms of a vector copula for a given partition of the random vector. Motivated by this result, vector copulas can be used to bind together multivariate marginals to create a joint density with inter-block dependence.

Whereas Fan and Henry (2023) use vector copula models in low dimensions to model data, we use them here in high dimensions as variational approximations. Two different flexible fixed form cyclically monotone transformations are considered to define the multivariate marginals of the blocks. These are coupled together by either a Gaussian vector copula (GVC) or Kendall vector copula (KVC) to specify dependent block variational posteriors. The GVC has a restricted form parameter matrix, for which we consider two characterizations: a factor pattern and an orthogonal pattern. Generative representations are given for these vector copula models, which are necessary to implement SGD algorithms with re-parameterized gradients for the efficient solution of the variational optimization.

To demonstrate the efficacy and broad applicability of our proposed VCVI method we employ it to estimate four example statistical models. The first is a logistic regression, with coefficients regularized using a horseshoe prior (Carvalho et al., 2010), for sparse signals from nine datasets with between 38 and 10,000 covariates. The second is a correlation matrix parameterized by spherical co-ordinates that are regularized using a Bayesian LASSO (Figueiredo, 2003), applied to an economic dataset with 49 variables and only 103 observations. The third is an unobserved component

stochastic volatility for U.S. inflation (Chan, 2017). The fourth is an additive p-spline model with a hierarchical prior for regression function smoothing (Lang and Brezger, 2004). In all four examples, it is attractive to partition the model parameters into blocks. We show that dependent block posteriors from VCVI are more accurate approximations than assuming inter-block independence. They also out-perform other benchmark variational approximations that capture dependence in the posterior without partitioning the parameters into blocks, including factor covariance Gaussians (Ong et al., 2018) and conventional Gaussian copulas (Han et al., 2016, Smith et al., 2020).

A few studies have considered dependent block posteriors for VI. Menictas et al. (2023) use different product restrictions in factorized VI to estimate a model with crossed random effects. They find that allowing global parameters to be correlated with random effects is important to estimate both of them accurately. Similarly, Goplerud et al. (2023) show that making fixed effects dependent on random effects in a generalized linear mixed model can improve estimation of the posterior in VI. Loaiza-Maya and Nibbering (2023) consider a Gaussian approximation with a parsimonious patterned covariance matrix for inter- and intra-block dependence exhibited by the posterior of a multinomial probit model. However, as far as we are aware, our study is the first to construct dependent block posterior approximations in VI in a general fashion using vector copulas.

The rest of the paper is organized as follows. Section 2 briefly introduces VI using SGD and copula models, and then outlines vector copula models and their use as variational approximations. Section 3 suggests vector copulas that are both attractive choices to capture dependence in blocked posteriors and also learnable using SGD with the re-parameterization trick. Section 4 contains the four example applications of VCVI, while Section 5 concludes.

2 Vector Copula Variational Inference

In this section we first review the basic concepts of VI and copula models, and then introduce vector copula models and their use as a variational approximation (VA).

2.1 Variational Inference

Let $\boldsymbol{\theta} \in \mathbb{R}^d$ be a vector of unknown parameter values, possibly augmented with some latent variables, and \mathbf{y} be observed data. VI approximates the posterior $p(\boldsymbol{\theta}|\mathbf{y}) \propto p(\mathbf{y}|\boldsymbol{\theta})p(\boldsymbol{\theta}) \equiv h(\boldsymbol{\theta})$, where $p(\mathbf{y}|\boldsymbol{\theta})$ is the likelihood and $p(\boldsymbol{\theta})$ is the prior density, by a VA with density $q(\boldsymbol{\theta}) \in \mathcal{Q}$. To learn the VA it is common to minimize the Kullback-Leibler divergence (KLD) between $q(\boldsymbol{\theta})$ and $p(\boldsymbol{\theta}|\mathbf{y})$. This is equivalent to maximizing the evidence lower bound (ELBO) (Ormerod and Wand, 2010)

$$\mathcal{L}(q) = \int \log \frac{h(\boldsymbol{\theta})}{q(\boldsymbol{\theta})} q(\boldsymbol{\theta}) d\boldsymbol{\theta} = \mathbb{E}_q (\log h(\boldsymbol{\theta}) - \log q(\boldsymbol{\theta})) , \quad (1)$$

over $q \in \mathcal{Q}$ which is called the variational optimization.

Key to effective VI is the selection of a distributional family \mathcal{Q} that provides an accurate approximation, while also allowing fast solution of the variational optimization. When $q(\boldsymbol{\theta})$ is parameterized by $\boldsymbol{\lambda}$ (a so-called “fixed form” VA) we write the density as $q_\lambda(\boldsymbol{\theta})$ and solve the optimization problem by SGD combined with the “re-parameterization trick” (Kingma and Welling, 2013, Rezende et al., 2014). This trick draws a random vector $\boldsymbol{\epsilon} \sim f_\epsilon$, such that $\boldsymbol{\theta} = g(\boldsymbol{\epsilon}, \boldsymbol{\lambda}) \sim q_\lambda$ for a deterministic function g , so that (1) can be written as

$$\mathcal{L}(\boldsymbol{\lambda}) = \mathbb{E}_{f_\epsilon} (\log h(g(\boldsymbol{\epsilon}, \boldsymbol{\lambda})) - \log q_\lambda(g(\boldsymbol{\epsilon}, \boldsymbol{\lambda}))) , \quad (2)$$

where we now write the ELBO as a function of $\boldsymbol{\lambda}$. Differentiating under the integral in (2) gives:

$$\nabla_{\boldsymbol{\lambda}} \mathcal{L}(\boldsymbol{\lambda}) = \mathbb{E}_{f_\epsilon} \left\{ \left[\frac{dg(\boldsymbol{\epsilon}, \boldsymbol{\lambda})}{d\boldsymbol{\lambda}} \right]^\top \nabla_{\boldsymbol{\theta}} (\log h(\boldsymbol{\theta}) - \log q_\lambda(\boldsymbol{\theta})) \right\} . \quad (3)$$

For careful choices of q_λ , f_ϵ and g , a Monte Carlo estimate of the expectation in (3) has low variability (Xu et al., 2019). Usually, only one draw $\boldsymbol{\epsilon} \sim f_\epsilon$ is sufficient, making optimization using SGD fast. The elements of $\boldsymbol{\lambda}$ are either unconstrained or transformed to be so.¹ In addition, it is not necessary for $\boldsymbol{\lambda}$ to be uniquely identified.

For complex and/or large statistical models it is popular to partition $\boldsymbol{\theta} = (\boldsymbol{\theta}_1^\top, \boldsymbol{\theta}_2^\top, \dots, \boldsymbol{\theta}_M^\top)^\top$ and assume independence between blocks, so that $q(\boldsymbol{\theta}) = \prod_{j=1}^M q_j(\boldsymbol{\theta}_j)$. This is called a factorized or

¹While we do not explicitly mention these transformations in the rest of the text, we replace λ_i with $\tilde{\lambda}_i \in \mathbb{R}$ in the following circumstances: (i) if $\lambda_i > 0$ we set $\lambda_i = \tilde{\lambda}_i^2$, and (ii) if $\lambda_i \in (a, b)$ we set $\lambda_i = a + (b - a)/(1 + \exp(-\tilde{\lambda}_i))$.

mean field approximation, and it simplifies solution of the optimization (e.g. using fast coordinate ascent algorithms as in [Ormerod and Wand \(2010\)](#)) while allowing selection of approximations q_j to match the marginal posteriors $p(\boldsymbol{\theta}_j|\mathbf{y})$. However, in practice the suitability of this independence assumption is rarely considered. In this paper we use a vector copula model for q to allow for tailored marginals q_j , while also introducing posterior dependence between the blocks. We show how to use SGD with re-parameterization gradients at (3) to provide fast solution of the optimization.

2.2 Conventional copula models

Before introducing vector copulas, we briefly outline conventional copula models and their use as VAs. These are motivated by Sklar’s theorem, which represents a distribution by its univariate marginals and a copula function ([Nelsen, 2006](#), pp.42-43). For continuous $\boldsymbol{\theta} = (\theta_1, \dots, \theta_d)^\top$, a copula model has density

$$q(\boldsymbol{\theta}) = c(F_1(\theta_1), \dots, F_d(\theta_d)) \prod_{i=1}^d q_i(\theta_i), \quad (4)$$

where F_i and $q_i = \frac{\partial F_i}{\partial \theta_i}$ are marginal distribution and density functions of θ_i , respectively, and $c(\mathbf{u})$ is a density function on $\mathbf{u} = (u_1, \dots, u_d)^\top \in [0, 1]^d$ with uniform marginals, called the copula density. A copula model is a flexible way of constructing a multivariate distribution through choice of c and q_1, \dots, q_d ; see [Nelsen \(2006\)](#) and [Joe \(2014\)](#) for introductions.

[Tran et al. \(2015\)](#), [Han et al. \(2016\)](#), [Smith et al. \(2020\)](#), [Smith and Loaiza-Maya \(2023\)](#) and [Gunawan et al. \(2024\)](#) use copula models as VAs. However, evaluation of the gradient $\nabla_{\boldsymbol{\theta}} \log q(\boldsymbol{\theta})$ in (3) can be too slow for some choices of copula c and/or marginals q_i . To solve this problem, [Smith and Loaiza-Maya \(2023\)](#) construct copula models by element-wise monotonic transformations $\theta_i = t_i(u_i)$, so that $q_i(\theta_i) = \frac{\partial t_i^{-1}(\theta_i)}{\partial \theta_i}$ and $u_i = F_i(\theta_i) = t_i^{-1}(\theta_i)$ at (4). For example, for an elliptical copula ([Frahm et al., 2003](#)) these authors use the learnable transformations

$$\theta_i = t_i(u_i) \equiv b_i + s_i \cdot k_{\boldsymbol{\eta}_i} \left(F_e^{-1}(u_i) \right), \quad \text{for } i = 1, 2, \dots, d. \quad (5)$$

Here, b_i and s_i capture the mean and scale of θ_i , respectively, F_e^{-1} is the quantile function of a univariate standardized elliptical distribution (e.g. Φ^{-1} for the Gaussian), and $k_{\boldsymbol{\eta}_i}$ is a monotone

function with parameters $\boldsymbol{\eta}_i$ that captures the marginal asymmetry of θ_i . For careful choices of $k_{\boldsymbol{\eta}_i}$, evaluation of the required gradient is fast. We show in Section 2.4 that a generalization of this transformation approach can also be used to specify vector copula models as VAs.

2.3 Vector copula models

Sklar’s theorem is strictly defined for univariate marginals, and it is impossible to simply replace the arguments of the copula density in (4) with multivariate marginals F_j ; see Genest et al. (1995), Ressel (2019). However, in recent work Fan and Henry (2023) developed the idea of a vector copula that is based on an extension of Sklar’s theorem, as we now outline.

Consider the partition $\boldsymbol{\theta} = (\boldsymbol{\theta}_1^\top, \dots, \boldsymbol{\theta}_M^\top)^\top$, where $\boldsymbol{\theta}_j \in \mathbb{R}^{d_j}$ and $d = d_1 + \dots + d_M$. An M -block vector copula C_v is a distribution function on $[0, 1]^d$ with multivariate uniform marginal distributions μ_j on $[0, 1]^{d_j}$, for $j = 1, \dots, M$. There is no “within dependence” in μ_j , but C_v captures “between dependence” of the M blocks. Theorem 1 of Fan and Henry (2023) gives the vector extension of Sklar’s theorem, and we focus on its use to construct a probability distribution. For an M -block vector copula C_v with marginals μ_1, \dots, μ_M , P is a distribution on $\mathbb{R}^{d_1} \times \dots \times \mathbb{R}^{d_M}$ with marginal distributions P_j on \mathbb{R}^{d_j} if each P_j is a push-forward measure from μ_j by a transformation $\nabla\psi_j : [0, 1]^{d_j} \rightarrow \mathbb{R}^{d_j}$, where $\nabla\psi_j$ is the gradient of a convex function. Moreover, if each marginal P_j is absolutely continuous with density q_j , then the density function of P is

$$\begin{aligned} q(\boldsymbol{\theta}) &= c_v(\nabla\psi_1^*(\boldsymbol{\theta}_1), \dots, \nabla\psi_M^*(\boldsymbol{\theta}_M)) \prod_{j=1}^M q_j(\boldsymbol{\theta}_j) \\ &= c_v(\mathbf{u}_1, \dots, \mathbf{u}_M) \prod_{j=1}^M q_j(\boldsymbol{\theta}_j), \end{aligned} \tag{6}$$

where ψ_j^* is the convex conjugate of ψ_j , $\mathbf{u}_j = \nabla\psi_j^*(\boldsymbol{\theta}_j) \in [0, 1]^{d_j}$, $\mathbf{u} = (\mathbf{u}_1^\top, \dots, \mathbf{u}_M^\top)^\top$ and $c_v(\mathbf{u}) = \frac{\partial^d}{\partial u_1 \dots \partial u_d} C_v(\mathbf{u})$ is an M -block vector copula density. For absolutely continuous P , $\nabla\psi_j^* = (\nabla\psi_j)^{-1}$, which is the case when we use (6) as a VA.

An important observation is that the gradient of a convex function is a cyclically monotone function, and vice versa. A cyclically monotone function generalizes the idea of monotonicity to

multivariate functions and is defined as follows. A function $T : \mathbb{R}^{d_j} \rightarrow \mathbb{R}^{d_j}$ is cyclically monotone if for any finite sequence of points $\mathbf{x}_1, \mathbf{x}_2, \dots, \mathbf{x}_k$ in its domain, $\sum_{i=1}^k T(\mathbf{x}_i)^\top (\mathbf{x}_{i+1} - \mathbf{x}_i) \leq 0$ and $\mathbf{x}_{k+1} = \mathbf{x}_1$ to complete the cycle. Moreover, compositions of cyclically monotone functions are also cyclically monotone. This motivates the construction of multivariate marginals from such functions as we discuss below.

2.4 Multivariate marginal approximations

Let the cyclically monotone function $T_j^* \equiv \nabla \psi_j^*$ have inverse² T_j , which is therefore also cyclically monotone. In a vector copula model, $\mathbf{u} = (\mathbf{u}_1^\top, \dots, \mathbf{u}_M^\top)^\top \sim C_v$ (so that $\mathbf{u}_j \sim \mu_j$ is uniformly distributed) and $\boldsymbol{\theta}_j = T_j(\mathbf{u}_j)$ is a transformation that recovers the within dependence for block j . Thus, selection of transformation T_j determines the multivariate marginal of $\boldsymbol{\theta}_j$. By considering a change of variables from $\boldsymbol{\theta}_j$ to \mathbf{u}_j , the marginal density

$$q_j(\boldsymbol{\theta}_j) = \left| \det \left\{ \frac{\partial T_j^*}{\partial \boldsymbol{\theta}_j} \right\} \right|.$$

Two suitable cyclically monotone transformations T_j that provide a great deal of flexibility in constructing q_j are discussed below. Learnable vector copulas are discussed separately in Section 3.

The first transformation is a generalization of that at (5) to the multivariate case, and is similar to that used by [Salomone et al. \(2023\)](#):

$$\text{M1} : \quad T_j(\mathbf{u}_j) = \mathbf{b}_j + S_j \underline{k}_{\boldsymbol{\eta}_j} \{L_j \underline{\Phi}^{-1}(\mathbf{u}_j)\}. \quad (7)$$

Here, \mathbf{b}_j captures location, S_j is a diagonal matrix with positive elements to capture scale, and L_j is a lower triangular matrix with ones on its diagonal to captures within dependence. The function $\underline{\Phi}^{-1}(\mathbf{u}_j)$ is the standard Gaussian quantile function applied element-wise to \mathbf{u}_j . If $\mathbf{x}_j = (x_1, \dots, x_{d_j})^\top$ and $\boldsymbol{\eta}_j = (\boldsymbol{\eta}_{j,1}^\top, \dots, \boldsymbol{\eta}_{j,d_j}^\top)^\top$, then the function $\underline{k}_{\boldsymbol{\eta}_j}(\mathbf{x}_j) = (k_{\boldsymbol{\eta}_{j,1}}(x_1), \dots, k_{\boldsymbol{\eta}_{j,d_j}}(x_{d_j}))^\top$ with $k_{\boldsymbol{\eta}_{j,s}} : \mathbb{R} \rightarrow \mathbb{R}$ a monotonic function parameterized by $\boldsymbol{\eta}_{j,s}$. The variational parameters for marginal q_j are $\boldsymbol{\lambda}_j = (\mathbf{b}_j^\top, \text{diag}(S_j)^\top, \text{vech}(L_j)^\top, \boldsymbol{\eta}_j^\top)^\top$, where $\text{vech}(L_j)$ denotes the half-vectorization of L_j for only the non-fixed lower triangular elements. We refer to the transformation at (7) and

²We only consider invertible cyclically monotone functions in this paper.

its resulting marginal distribution as “M1”.

For k_η we use the inverse of the YJ transformation (Yeo and Johnson, 2000), which is parameterized by a scalar $0 < \eta < 2$, such that

$$k_\eta(x) = \begin{cases} 1 - (1 - x(2 - \eta))^{\frac{1}{2-\eta}} & \text{if } x < 0, \\ (1 + x\eta)^{\frac{1}{\eta}} - 1 & \text{if } x \geq 0, \end{cases} \quad (8)$$

and equals the identity transformation $k_\eta(x) = x$ when $\eta = 1$. Smith et al. (2020) show this transformation is effective in capturing skewed marginals in θ_i , although other choices for k_η include the G&H transformation of Tukey (Headrick et al., 2008) and the inverse of the sinh-arcsinh transformation of Jones and Pewsey (2009) used by Salomone et al. (2023).

As we demonstrate later, an attractive feature of M1 is that a pattern may be adopted for L_j that is a suitable for $p(\boldsymbol{\theta}_j|\mathbf{y})$, reducing the number of variational parameters $\boldsymbol{\lambda}_j$ and improving performance of the SGD algorithm when d_j is high. For example, in our empirical work we constrain L_j to be diagonal when within dependence of $\boldsymbol{\theta}_j$ is close to zero, and L_j^{-1} to be a band matrix when an ordering of the elements of $\boldsymbol{\theta}_j$ is serially dependent.

When d_j is large and a patterned L_j is inappropriate, then we adopt the alternative cyclically monotone transformation

$$\text{M2 : } \quad T_j(\mathbf{u}_j) = \mathbf{b}_j + \underline{k}_{\boldsymbol{\eta}_j} (E_j \underline{\Phi}^{-1}(\mathbf{u}_j)). \quad (9)$$

Here, $E_j = J_j J_j^T + D_j^2$, where J_j is a $(d_j \times w)$ matrix with $w < d_j$, D_j is a diagonal matrix, and \mathbf{b}_j , $\underline{\Phi}^{-1}(\mathbf{u}_j)$, $\underline{k}_{\boldsymbol{\eta}_j}$ are as defined as before. When d_j is large and $w \ll d_j$ this transformation captures within dependence more parsimoniously than does M1 with dense L_j . This variational parameters are $\boldsymbol{\lambda}_j = (\mathbf{b}_j^\top, \text{vec}(J_j), \text{diag}(D_j), \boldsymbol{\eta}_j^\top)^\top$, and the dimension of $\boldsymbol{\lambda}_j$ increases only linearly with d_j . The determinant and inverse of E_j can be computed efficiently by the Woodbury formula, which is necessary when evaluating the gradient of q . We refer to this transformation and its resulting marginal distribution as “M2”.

We make five observations on these multivariate marginals. First, when the identity transforma-

tion is employed (i.e. where $\eta = 1$ in equation (8) for each element) then M1 and M2 correspond to multivariate Gaussians $\boldsymbol{\theta}_j \sim N(\mathbf{b}_j, S_j L_j L_j^\top S_j)$ and $\boldsymbol{\theta}_j \sim N(\mathbf{b}_j, E_j E_j^\top)$, respectively. Second, when $\boldsymbol{\eta}_j$ is learned from the data, then M1 and M2 correspond to Gaussian copula models with flexible skewed marginals as shown in [Smith et al. \(2020\)](#). Third, if $\underline{\Phi}^{-1}$ is replaced in (7) and (9) with the element-wise application of the quantile function of another elliptical distribution, then M1 and M2 correspond to the elliptical copula model ([Smith and Loaiza-Maya, 2023](#)). Fourth, other learnable cyclically monotone transformations can also be used here. For example, [Bryan et al. \(2021\)](#) list some other cyclically monotone functions, while learnable cyclically monotone transport maps are also promising choices; e.g. see ([Makkuva et al., 2020](#)). The fifth observation is that M1 and M2 are types of (cyclically monotone) normalizing flows ([Papamakarios et al., 2021](#)) with Gaussian base distribution $\mathbf{z}_j = \underline{\Phi}^{-1}(\mathbf{u}_j) \sim N(\mathbf{0}, I_{d_j})$. Normalizing flows are employed widely as effective distributional approximations, as we find for M1 and M2.

Finally we note that when $d_j = 1$, the cyclically monotone transformation $\nabla\psi_j^*$ is the monotone distribution function F_j , and the density at (4) equals that at (6), so that the vector copula model nests the conventional copula model. Moreover, constructing the multivariate marginal by selecting a learnable cyclically monotone function T_j generalizes the construction of a univariate marginal of θ_i by selecting a learnable monotone function t_i as in Section 2.2.

2.5 Variational optimization

We evaluate (2) using the re-parameterization trick with g given by the composition of two functions. The first is $\mathbf{u} = g_1(\boldsymbol{\epsilon}, \boldsymbol{\lambda}_{\text{vc}}) \sim C_v$, where $\boldsymbol{\epsilon} \sim f_\epsilon$ and $\boldsymbol{\lambda}_{\text{vc}}$ are the vector copula parameters, which is specified separately for different vector copulas in Section 3. The second function is $g_2(\mathbf{u}, \boldsymbol{\lambda}_{\text{marg}}) = (T_1(\mathbf{u}_1; \boldsymbol{\lambda}_1)^\top, \dots, T_M(\mathbf{u}_M; \boldsymbol{\lambda}_M)^\top)^\top$, where $\boldsymbol{\lambda}_{\text{marg}} = (\boldsymbol{\lambda}_1^\top, \dots, \boldsymbol{\lambda}_M^\top)^\top$ denotes the parameters of all M marginals. Then setting $\boldsymbol{\lambda} = (\boldsymbol{\lambda}_{\text{vc}}^\top, \boldsymbol{\lambda}_{\text{marg}}^\top)^\top$, the transformation is

$$\boldsymbol{\theta} = g(\boldsymbol{\epsilon}, \boldsymbol{\lambda}) \equiv g_2(g_1(\boldsymbol{\epsilon}, \boldsymbol{\lambda}_{\text{vc}}), \boldsymbol{\lambda}_{\text{marg}}).$$

Algorithm 1 : *Vector Copula Variational Inference (VCVI) with Re-parameterized Gradient*

Set $s = 0$ and initialize $\boldsymbol{\lambda}^{(0)}$ to a feasible value

repeat

1. Generate $\boldsymbol{\epsilon}^{(s)} \sim f_{\boldsymbol{\epsilon}}$ and set $\mathbf{u} = g_1(\boldsymbol{\epsilon}, \boldsymbol{\lambda}_{\text{vc}}^{(s)})$.
2. Set $\boldsymbol{\theta}_j = T_j(\mathbf{u}_j; \boldsymbol{\lambda}_j^{(s)})$ for $j = 1, \dots, M$.
3. Evaluate gradient estimate $\widehat{\nabla_{\boldsymbol{\lambda}} \mathcal{L}(\boldsymbol{\lambda})}$ at $\boldsymbol{\lambda} = \boldsymbol{\lambda}^{(s)}$.
4. Update $\boldsymbol{\lambda}^{(s+1)} = \boldsymbol{\lambda}^{(s)} + \boldsymbol{\rho}_s \circ \widehat{\nabla_{\boldsymbol{\lambda}} \mathcal{L}(\boldsymbol{\lambda}^{(s)})}$ where $\boldsymbol{\rho}_s$ is a vector of adaptive step sizes.
5. Set $s = s + 1$.

until Either a stopping rule is satisfied or a fixed number of steps is taken.

Algorithm 1 gives the VCVI algorithm. At Step 3 an unbiased estimate of the re-parameterized gradient at (3) is obtained by replacing $\boldsymbol{\epsilon}$ (therefore also $\boldsymbol{\theta} = g(\boldsymbol{\epsilon}, \boldsymbol{\lambda})$) by its single drawn value $\boldsymbol{\epsilon}^{(s)}$. In Step 4, “ \circ ” denotes the Hadamard (i.e. element-wise) product, and $\boldsymbol{\rho}_s$ is the vector of adaptive step sizes determined automatically using an ADA algorithm, such as ADAM (Kingma and Ba, 2014) or ADADELTA (Zeiler, 2012).

3 Learnable Vector Copulas

Fan and Henry (2023) consider vector copulas for modeling data, and this section outlines two that are suitable for VCVI: the Gaussian (GVC) and Kendall (KVC) vector copulas. Consistent with Section 2.3, these are defined for M blocks of dimension $d = \sum_{j=1}^M d_j$ on $\mathbf{u} = (\mathbf{u}_1^\top, \dots, \mathbf{u}_M^\top)^\top$ with $\mathbf{u}_j = (u_{j,1}, u_{j,2}, \dots, u_{j,d_j})^\top \in [0, 1]^{d_j}$. We propose parameterizations of these vector copulas that can provide accurate approximations and allow the variational optimization to be solved efficiently.

3.1 Gaussian vector copula

The GVC has distribution function

$$C_v^{Ga}(\mathbf{u}_1, \dots, \mathbf{u}_M; \Omega) \equiv \Phi_d(\underline{\Phi}^{-1}(\mathbf{u}_1), \dots, \underline{\Phi}^{-1}(\mathbf{u}_M); \Omega) . \quad (10)$$

Here, $\underline{\Phi}^{-1}$ denotes element-wise application of the standard normal quantile function, and $\Phi_d(\cdot; \Omega)$ is the distribution function of a d -dimensional zero mean normal with correlation Ω . Unlike a conventional Gaussian copula, C_v^{Ga} captures no within dependence in each block. The correlation

matrix Ω has identity matrices $I_{d_1}, I_{d_2}, \dots, I_{d_M}$ on its leading diagonal, and we denote the set of such patterned correlation matrices as \mathcal{P} . Differentiating (10) with respect to \mathbf{u} gives the density

$$c_v^{Ga}(\mathbf{u}_1, \dots, \mathbf{u}_M; \Omega) = \det(\Omega)^{-1/2} \exp \left\{ -\frac{1}{2} \underline{\Phi}^{-1}(\mathbf{u})^\top (\Omega^{-1} - I_d) \underline{\Phi}^{-1}(\mathbf{u}) \right\}. \quad (11)$$

As with the conventional Gaussian copula, to sample \mathbf{u} from (10), draw $\mathbf{z} \sim N_d(\mathbf{0}, \Omega)$, then set $\mathbf{u} = \underline{\Phi}(\mathbf{z})$ which denotes the standard Gaussian distribution function applied element-wise to \mathbf{z} .

The main challenge in employing the GVC as a VA is to specify an appropriate parameterization of $\Omega \in \mathcal{P}$. To be an effective VA when d is large, the parameterization needs to (i) be parsimonious, (ii) allow application of the re-parameterization trick for fast optimization using SGD, and (iii) enable efficient evaluation of Ω^{-1} and $\det(\Omega)$ when computing (11) and its derivatives. Two such parameterizations of Ω are now given.

3.1.1 Factor pattern correlation matrix

The first parameterization was suggested by Ren et al. (2019) in a different context. For a scalar $\zeta > 0$ and a $(d \times p)$ matrix B with $p < d$, let

$$\tilde{\Omega} = \zeta I_d + BB^\top, \quad \text{and} \quad \Omega = A\tilde{\Omega}A^\top.$$

Here, $A = [\text{bdiag}(\tilde{\Omega})]^{-1/2}$ is the inverse of the lower triangular Cholesky factor of the matrix $\text{bdiag}(\tilde{\Omega})$, which in turn denotes a block diagonal matrix with blocks of sizes d_1, \dots, d_M comprising the same elements as $\tilde{\Omega}$ (i.e. this operator simply returns $\tilde{\Omega}$, but with all blocks on the main diagonal to be identity matrices). It is easy to show that $\Omega \in \mathcal{P}$. This is a factor patterned correlation matrix that captures between dependence based on a low-rank representation when $p \ll d$.

It is straightforward to generate $\mathbf{z} \sim N_d(\mathbf{0}, \Omega)$ using the decomposition $\Omega = A(\zeta I_d + BB^\top)A^\top = \zeta AA^\top + ABB^\top A^\top$ as follows. Draw independent normals $\boldsymbol{\epsilon} = (\boldsymbol{\epsilon}_1^\top, \boldsymbol{\epsilon}_2^\top)^\top \sim N_{d+p}(\mathbf{0}, I_{d+p})$, and set

$$\mathbf{z} = \zeta^{1/2} A\boldsymbol{\epsilon}_1 + A\boldsymbol{\epsilon}_2 = \underline{\Phi}^{-1}(g_1(\boldsymbol{\epsilon}, \boldsymbol{\lambda}_{\text{vc}})). \quad (12)$$

with $\boldsymbol{\lambda}_{\text{vc}} = (\zeta, \text{vec}(B)^\top)^\top$. Equation (12) also provides the specification of g_1 for implementation of the re-parameterization trick. The inverse $\Omega^{-1} = A^{-T}\tilde{\Omega}^{-1}A^{-1}$, where $\tilde{\Omega}^{-1}$ can be computed effi-

ciently using the Woodbury formula, and A^{-1} can be evaluated using p sequential rank-1 Cholesky factor updates.³ We label the GVC with this factor patterned Ω with p factors as ‘‘GVC-F p ’’.

3.1.2 Orthogonal pattern correlation matrix

The second parameterization of Ω was suggested by Bryan et al. (2021) in a different context for $M = 2$ blocks, where

$$\Omega = \begin{bmatrix} I_{d_1} & Q_1 \Lambda Q_2^\top \\ Q_2 \Lambda Q_1^\top & I_{d_2} \end{bmatrix}. \quad (13)$$

Here, Q_1, Q_2 are left semi-orthogonal matrices with dimensions $(d_1 \times \tilde{d})$ and $(d_2 \times \tilde{d})$, respectively, $\tilde{d} = \min(d_1, d_2)$, and $\Lambda = \text{diag}(l_1, \dots, l_{\tilde{d}})$ is a $(\tilde{d} \times \tilde{d})$ diagonal matrix. Thus, $Q_1^\top Q_1 = Q_2^\top Q_2 = I_{\tilde{d}}$. Without loss of generality, assume $d_1 \geq d_2$, so that $\tilde{d} = d_2$ and Q_2 is a square orthonormal matrix. Because Ω is a correlation matrix, then $0 < \det(\Omega) < 1$. The determinant of (13) can be used to identify constraints on Λ that ensures $\Omega \in \mathcal{P}$ as follows. Let $\Omega/I_{d_1} = I_{d_2} - Q_2 \Lambda Q_1^\top I_{d_1}^{-1} Q_1 \Lambda Q_2^\top = I_{d_2} - Q_2 \Lambda^2 Q_2^\top$ be the Schur complement of block I_{d_1} in the matrix Ω . Then,

$$\begin{aligned} \det(\Omega) &= \det(I_{d_1}) \cdot \det(\Omega/I_{d_1}) = \det(I_{d_2} - Q_2 \Lambda^2 Q_2^\top) \\ &= \det(Q_2 (I_{\tilde{d}} - \Lambda^2) Q_2^\top) = \det(I_{\tilde{d}} - \Lambda^2) = \prod_{i=1}^{\tilde{d}} (1 - l_i^2). \end{aligned}$$

Thus, a sufficient condition to ensure $\Omega \in \mathcal{P}$ is to restrict $|l_i| < 1$ for $i = 1, \dots, \tilde{d}$.

The matrix can be factorized as $\Omega = \Omega_L \Omega_L^\top$, where

$$\Omega_L = \begin{bmatrix} I_{d_1} & \mathbf{0}_{d_1 \times d_2} \\ Q_2 \Lambda Q_1^\top & Q_2 \sqrt{I_{\tilde{d}} - \Lambda^2} \end{bmatrix},$$

$\mathbf{0}_{d_1 \times d_2}$ is a $(d_1 \times d_2)$ matrix of zeros, and Ω_L is a parsimonious (non-Cholesky) factor. To generate $\mathbf{z} \sim N_d(\mathbf{0}, \Omega)$ first draw independent normals $\boldsymbol{\epsilon} = (\boldsymbol{\epsilon}_1^\top, \boldsymbol{\epsilon}_2^\top)^\top \sim \mathcal{N}_{d_1+d_2}(0, I)$, and then set

$$\mathbf{z} = \Omega_L \boldsymbol{\epsilon} = \Phi^{-1}(g_1(\boldsymbol{\epsilon}, \boldsymbol{\lambda}_{\text{vc}})), \quad (14)$$

³By the Woodbury formula, $\tilde{\Omega}^{-1} = \frac{1}{\zeta} [I_d - B(\frac{1}{\zeta} I_p + B^\top B)^{-1} B^\top]$ requiring inversion of only a $p \times p$ matrix. To compute the Cholesky factor A^{-1} note that $\zeta I_d + B B^\top = \zeta I_d + \mathbf{b}_1 \mathbf{b}_1^\top + \dots + \mathbf{b}_p \mathbf{b}_p^\top$ where \mathbf{b}_i is the i th column of B , so its Cholesky factor can be computed using p sequential rank-1 updates, each of $O(d^2)$.

which also specifies the transformation g_1 with $\boldsymbol{\lambda}_{\text{vc}} = (\boldsymbol{l}^\top, \text{vec}(Q_1), \text{vec}(Q_2))^\top$, where $\boldsymbol{l} = (l_1, \dots, l_{\bar{d}})^\top$.

The inverse of Ω has the analytical expression

$$\Omega^{-1} = \begin{bmatrix} I_{d_1} + Q_1 \Lambda (I_{\bar{d}} - \Lambda^2)^{-1} \Lambda Q_1^\top & -Q_1 \Lambda (I_{\bar{d}} - \Lambda^2)^{-1} Q_2^\top \\ -Q_2 (I_{\bar{d}} - \Lambda^2)^{-1} \Lambda Q_1^\top & Q_2 (I_{\bar{d}} - \Lambda^2)^{-1} Q_2^\top \end{bmatrix},$$

which is fast to compute because $I_{\bar{d}} - \Lambda^2$ is a diagonal matrix; see Part B of the Online Appendix.

Because the Schur complement is only applicable to a 2×2 partitioned matrix, it is difficult to extend this representation to more than $M = 2$ blocks. We label a GVC with this orthogonal pattern as ‘‘GVC-O’’. For some posteriors we also consider the special case where $Q_1 = Q_2 = I$ (so that only Λ parameterizes the off-diagonal blocks at (13)) and label this as ‘‘GVC-I’’.

3.2 Kendall vector copula

A Kendall vector copula (KVC) is a special case of the hierarchical Kendall copula suggested by Brechmann (2014). In a hierarchical Kendall copula, the within dependence of block j is captured by a ‘‘cluster copula’’ C_j , and the dependence between different blocks is controlled by an M -dimensional ‘‘nesting copula’’ C_0 . A general hierarchical Kendall copula is difficult to compute, but it is tractable for the special case of a KVC where the cluster copulas are independence copulas (i.e. $C_j(\mathbf{u}_j) = \prod_{s=1}^{d_j} u_{j,s}$ for $j = 1, \dots, M$). Let $c_0(\mathbf{v}; \boldsymbol{\lambda}_{\text{vc}}) = \frac{\partial^M}{\partial \mathbf{v}} C_0(\mathbf{v}; \boldsymbol{\lambda}_{\text{vc}})$ be the density of the nesting copula with $\mathbf{v} = (v_1, \dots, v_M)^\top$. Then, from Brechmann (2014, p.87), the density of the M -block KVC is

$$c_v^{KV}(\mathbf{u}_1, \dots, \mathbf{u}_M; \boldsymbol{\lambda}_{\text{vc}}) = c_0(\mathbf{v}; \boldsymbol{\lambda}_{\text{vc}}),$$

where $v_j = K_j(C_j(\mathbf{u}_j))$ for $j = 1, \dots, M$. Here, K_j is the distribution function of the random variable $V_j \equiv C_j(\mathbf{u}_j)$, which is called the Kendall distribution function. For the KVC, $K_j(t) = \sum_{b=0}^{d_j-1} \frac{t(-\ln t)^b}{b!}$, which is derived in Appendix B and can be computed efficiently using Horner’s method.

The between dependence of a KVC can be specified using a latent vector $\mathbf{R} = (R_1, \dots, R_M)^\top$ with the marginal distribution for each $R_j \geq 0$ given by an Erlang distribution with scale 1, shape

d_j and distribution function

$$F_{R_j}(r_j) = 1 - \sum_{b=0}^{d_j-1} \frac{r_j^b \exp(-r_j)}{b!}, \quad r_j \in [0, \infty).$$

This gives a generative procedure for the KVC with nesting copula C_0 outlined in Algorithm 2 below, with a derivation given in Appendix B.

Algorithm 2 Generation from an M -block KVC

Draw $\mathbf{v} = (v_1, \dots, v_M)^\top \sim C_0(\cdot; \boldsymbol{\lambda}_{\text{vc}})$, where $\boldsymbol{\lambda}_{\text{vc}}$ are the nesting copula parameters

for $j = 1 : M$ **do**

1. Set $r_j = F_{R_j}^{-1}(1 - v_j)$.
2. Draw d_j independent samples $\mathbf{e}_j = (e_{j,1}, \dots, e_{j,d_j})^\top$ from $\text{Exp}(1)$.
3. Set $\mathbf{s}_j = \frac{\mathbf{e}_j}{\|\mathbf{e}_j\|}$, where $\|\cdot\|$ is the L^1 norm.
4. Set $\mathbf{u}_j = \exp(-r_j \mathbf{s}_j)$.

end for

Then $\mathbf{u} = (\mathbf{u}_1^\top, \dots, \mathbf{u}_M^\top)^\top \sim C_v^{KV}$ with nesting copula C_0 and parameters $\boldsymbol{\lambda}_{\text{vc}}$

Any existing parametric copula can be used for C_0 , making the KVC as attractive as a VA. In our empirical work we employ a Gaussian copula with correlation matrix $\Omega_0 = \tilde{G}\tilde{G}^\top$ for $\tilde{G} = \text{diag}(GG^\top)^{-1/2}G$, with G a lower triangular positive definite matrix. Thus, \tilde{G} is a Cholesky factor, the leading diagonal elements of G are unconstrained positive real numbers, and $\boldsymbol{\lambda}_{\text{vc}} = \text{vech}(G)$. This full rank parameterization of Ω_0 is suitable for small to medium values of M (typically $M < 50$), although other full rank (Tan and Nott, 2018) or reduced rank (Ong et al., 2018) parameterizations for Ω_0 may also be used.

An expression for the re-parameterization transformation g_1 is obtained directly from Algorithm 2 as follows. Generate $\boldsymbol{\epsilon}_1 \sim N(\mathbf{0}, I_M)$ and d independent $e_{j,i} \sim \text{Exp}(1)$ random variables, then set $\boldsymbol{\epsilon} = (\boldsymbol{\epsilon}_1^\top, \mathbf{e}_1^\top, \dots, \mathbf{e}_M^\top)^\top$ with $\mathbf{e}_j = (e_{j,1}, \dots, e_{j,d_j})^\top$ for $j = 1, \dots, M$. The transformation is

$$\mathbf{u} = g_1(\boldsymbol{\epsilon}, \boldsymbol{\lambda}_{\text{vc}}) \equiv \exp \left\{ -\mathbf{r} \cdot \text{diag} \left(\frac{\mathbf{e}_1}{\|\mathbf{e}_1\|}, \dots, \frac{\mathbf{e}_M}{\|\mathbf{e}_M\|} \right) \right\},$$

where $\mathbf{r} = (F_{R_1}^{-1}(1 - v_1)\boldsymbol{\iota}_{d_1}, \dots, F_{R_M}^{-1}(1 - v_M)\boldsymbol{\iota}_{d_M})$ is a d dimension row vector, $\boldsymbol{\iota}_{d_j}$ is a d_j dimension row vector of ones, $\mathbf{v} = \underline{\Phi}(\tilde{G}\boldsymbol{\epsilon}_1)$, “diag(\mathbf{x})” denotes a diagonal matrix with leading diagonal elements \mathbf{x} , and the exponential function is applied element-wise. We label this Kendall vector copula with a

Gaussian nesting copula as “KVC-G”. Finally, we note that using a Gaussian copula for C_0 simplifies the re-parameterized gradients at (3) as discussed further in Part C of the Online Appendix.

3.3 Discussion of vector copulas

Table 1: Characteristics of Different Vector Copulas & Parameterizations

Vector Copula	M	Parameters	$\dim(\boldsymbol{\lambda}_{\text{vc}})$
GVC-F p	Unconstrained	ζ, B	$pd + 1$
GVC-O	2	Q_1, Q_2, Λ	$(d_1 + d_2 + 1)\tilde{d}$
GVC-I	2	Λ	\tilde{d}
KVC-G	Unconstrained	G	$M(M + 1)/2$

Note: p is the number of factors used in the GVC with factor patterned Ω ; d_1 and d_2 are the number of rows in Q_1 and Q_2 in the GVC with orthogonal patterned Ω ; and $\tilde{d} = \min(d_1, d_2)$.

Table 1 summarizes some of the characteristics of the vector copulas discussed above, and we make some comments on their suitability for capturing dependence between blocks in different posteriors. First, for GVC-F p the number of variational parameters $\dim(\boldsymbol{\lambda}_{\text{vc}})$ does not vary with the number of blocks M , so that this vector copula is attractive for partitions with large M . Second, the number of parameters of a KVC-G is determined by M and not d . In addition, blocks with large d_j incur minimal computational burden, making the KVC-G an attractive choice for high d , M and big blocks with large d_j . However, with a KVC dependence between blocks is captured by the M -dimensional nesting copula C_0 , which can prove limiting for some posteriors. For example, the KVC-G has only a single scalar parameter to capture dependence between each pair of blocks. Third, both GVC-O and GVC-I are restricted to two blocks. However, as we show in two examples, they are attractive to capture posterior dependence for popular local-global shrinkage priors. Moreover, they can be used as a marginal of other vector copula model when $M > 2$.

Finally, we note that any existing copula density with multivariate marginals that are independence copulas, are well-defined vector copulas. Therefore, the identification of additional vector copulas that prove suitable as VAs is a promising line of research.

4 Applications

To show the versatility of our method we apply it to estimate four different statistical models using 16 datasets, each with challenging posteriors. The first two models use global-local shrinkage priors, which result in posteriors that are approximated well using GVC-I. The second two models have correlated latent variables with a posterior for which GVC-F p and KVC-G are suitable approximations.

For comparison, we use the following (non-vector copula model) VAs as benchmarks:

- GMF: Fully factorized Gaussian mean field with d independent Gaussians.
- G-F p : Gaussian with a factor covariance structure with p factors as in [Ong et al. \(2018\)](#).
- GC-F p : Conventional Gaussian copula constructed by element-wise YJ transformations and a factor correlation matrix with p factors as in [Smith et al. \(2020\)](#).
- BLK: M independent blocks of either M1 or M2 ($w = 1$) multivariate Gaussian marginals (so that $\eta_{j,i} = 1$ for all i, j).
- BLK-C: As with BLK, except that $\boldsymbol{\eta}_1, \dots, \boldsymbol{\eta}_M$ are learned (so that each multivariate marginal is a Gaussian copula).

The SGD algorithm is used to calibrate all VAs. To ensure accurate results 40,000 steps are used, although the optimum is often reached within 5,000 steps in our examples. The VAs GC-F p and BLK-C have skewed univariate marginals, while G-F p and GC-F p capture dependence in $\boldsymbol{\theta}$ using p common sources of variation across all elements, and are among the best performing black-box VI methods that balance accuracy and speed for high d . Accuracy of a VA is measured using the ELBO at (1), computed as its median value over the final 1000 steps of the SGD algorithm. A higher ELBO value corresponds to a lower KLD between the VA and the target posterior.

We note that the first two models are difficult to estimate using MCMC for large datasets, and we show that VCVI is a fast and feasible alternative. The last two models can be estimated readily using MCMC, which allows the accuracy of VCVI to be demonstrated. The dimensions of the posteriors in our applications are listed in Table A2 in Part D of the Online Appendix.

4.1 Example 1: Sparse logistic regression with horseshoe regularization

The first application is a sparse logistic regression, where there is a large number of covariates m relative to the number of observations n . In this case it is usual to regularize the coefficient vector $\boldsymbol{\beta} = (\beta_1, \dots, \beta_m)^\top$, and here we use the horseshoe prior (Carvalho et al., 2010) given by

$$\beta_i | \xi, \delta_i \sim \mathcal{N}(0, \delta_i^2 \xi^2), \quad \delta_i \sim \mathcal{C}^+(0, 1), \quad \xi \sim \mathcal{C}^+(0, 1),$$

where \mathcal{C}^+ denotes the half-Cauchy distribution, δ_i is a local shrinkage parameter and ξ is the global shrinkage parameter. The posterior has a funnel-shaped posterior (Ghosh et al., 2018) that is hard to approximate and to simplify the geometry we use a non-centered parameterization (Ingraham and Marks, 2017) that sets $\beta_i = \alpha_i \delta_i \xi$ with prior $\alpha_i \sim \mathcal{N}(0, 1)$. The model parameters are $\boldsymbol{\theta} = (\boldsymbol{\alpha}^\top, \tilde{\boldsymbol{\delta}}^\top, \tilde{\xi})^\top$ where $\boldsymbol{\alpha} = (\alpha_1, \dots, \alpha_m)^\top$, $\tilde{\boldsymbol{\delta}} = (\tilde{\delta}_1, \dots, \tilde{\delta}_m)^\top$, $\tilde{\xi} = \log(\xi)$ and $\tilde{\delta}_i = \log(\delta_i)$.

We choose four lower dimensional datasets from Ong et al. (2018), named as *krkp*, *spam*, *iono*, *mushroom*. For the high-dimensional situation, we choose the dataset *cancer* from Ong et al. (2018) and the *QSAR Oral Toxicity* dataset from the UCI Machine Learning Repository. Additionally, we use the function “make_classification” from Scipy (Virtanen et al., 2020) to simulate three datasets with 5, 20 and 100 thousand observations, each with 10,000 covariates (with $\beta_i \neq 0$ for 2,000). The top rows of Table 2 lists these nine datasets and their size.

Two likely features of the posterior that guide our VA selection are that (i) the pairs $(\alpha_i, \tilde{\delta}_i)$ will be dependent, and (ii) when the signal is sparse (i.e. when the ratio n/m is low as in our datasets) within dependence in both $\boldsymbol{\alpha}$ and $\tilde{\boldsymbol{\delta}}$ is weak. We partition $\boldsymbol{\theta}$ into $(\boldsymbol{\alpha}^\top, \tilde{\boldsymbol{\delta}}^\top, \tilde{\xi})$ and consider the following 3-block vector copula models as VAs:

- A1/A2: GVC-F5 with marginals M1 ($L_j = I$) for all three blocks
- A3/A4: Bivariate GVC-I with marginals M1 ($L_j = I$) for $\boldsymbol{\alpha}$ and $\tilde{\boldsymbol{\delta}}$, and independent $\tilde{\xi}$
- A5/A6: Bivariate GVC-I with marginals M2 ($w = 1$) for $\boldsymbol{\alpha}$ and $\tilde{\boldsymbol{\delta}}$, and independent $\tilde{\xi}$

For approximations A1, A3 and A5 we set $k_{\boldsymbol{\eta}_j}$ to the identity transformation (i.e. where $\eta = 1$ in (8)) resulting in Gaussian marginals. For approximations A2, A4 and A6, $\boldsymbol{\eta}_1, \boldsymbol{\eta}_2, \boldsymbol{\eta}_3$ are learned, so that the two multivariate marginals for $\boldsymbol{\alpha}$ and $\tilde{\boldsymbol{\delta}}$ are conventional Gaussian copula models,

and all univariate marginals are potentially skewed. The benchmarks BLK/BLK-C have the same multivariate M2 marginals as A5/A6, but assume independence between all three blocks.

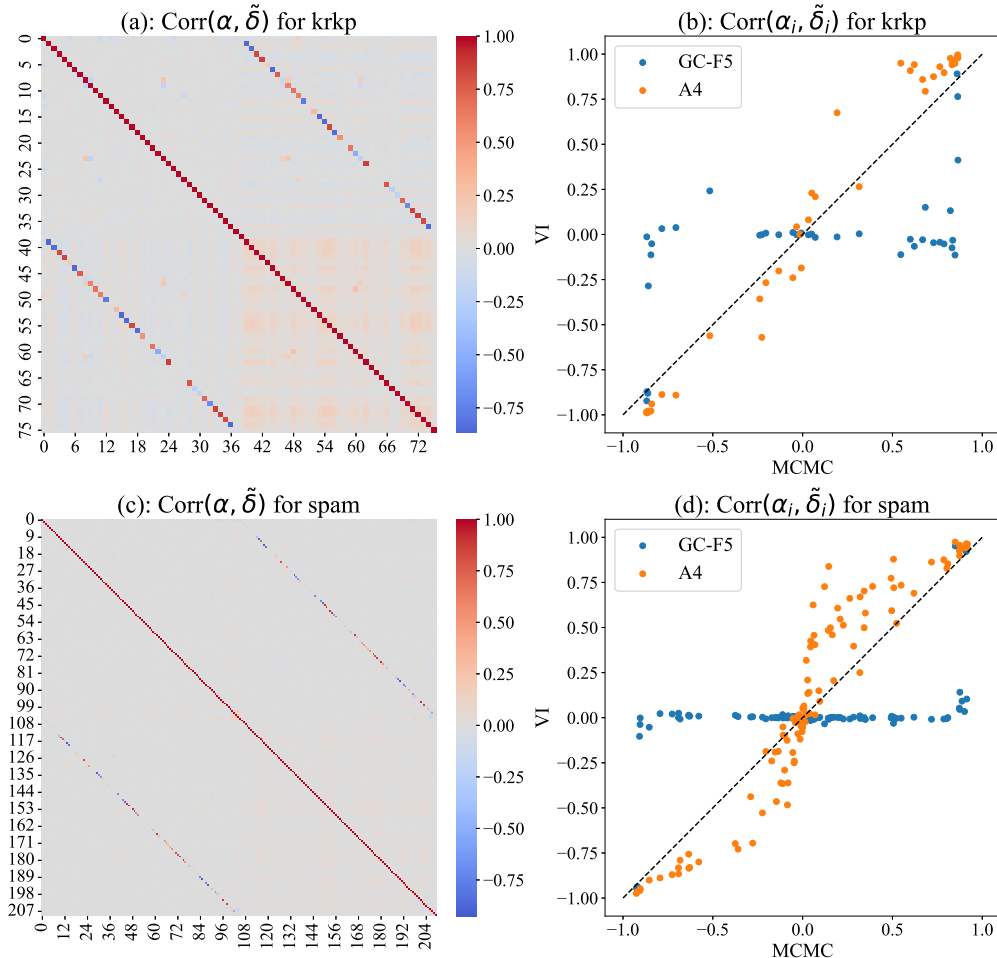


Figure 1: Posterior summaries for *krkp* (top row) and *spam* (bottom row). Panels (a,c) are heatmaps of the matrix of Spearman correlations for $(\alpha^\top, \tilde{\delta}^\top)$ computed exactly using (slow) MCMC. Panels (b,d) are scatterplots of $\{\text{corr}(\alpha_i, \tilde{\delta}_i); i = 1, \dots, m\}$, with exact posterior values on the horizontal axis, and variational approximations on the vertical axis for GC-F5 (blue dots) and A4 (orange dots).

Table 2 reports the ELBO value (computed as the median ELBO over the last 1000 steps of the SGD algorithm) for the GMF benchmark, and the difference between this and the values for the other VAs. We make five observations. First, allowing for dependence in the posterior in any way increases accuracy compared to GMF for all examples except the *cancer* dataset. This dataset is extreme, with only $n = 42$ observations on $m = 2001$ covariates, so that the prior dominates the likelihood in the posterior. Second, the popular G-Fp and GC-Fp (with either

Table 2: ELBO values for different VAs (rows) in the regularized logistic regression with nine datasets (columns)

Dataset	Low-Dimensional Real				High-dimensional Real				High-Dimensional Simulated			
	krkp	mushroom	spam	iono	cancer	qsar	simu1	simu2	simu3	simu1	simu2	simu3
Name	krkp	mushroom	spam	iono	cancer	qsar	simu1	simu2	simu3	simu1	simu2	simu3
Size (<i>n</i> x <i>m</i>)	3196x38	8124x96	4601x105	351x112	42x2001	8992x1024	5Kx10K	20Kx10K	100Kx10K	20Kx10K	20Kx10K	100Kx10K
<i>Benchmark VAs:</i>												
GMF	-382.01	-120.85	-856.77	-98.82	-77.59	-2245.10	-3641.64	-10844.22	-40735.67			
G-F5	8.69	1.44	5.76	2.35	-0.53	-11.18	-6.16	-18.47	-30.06			
GC-F5	11.43	10.96	15.52	7.05	-0.66	41.20	84.75	198.30	243.18			
G-F20	19.20	0.89	14.13	2.69	-1.92	-15.35	-25.68	-70.41	-167.53			
GC-F20	21.56	6.95	25.14	8.48	-2.02	18.35	65.13	153.44	119.17			
BLK	-3.13	0.42	-3.95	-6.28	-2.81	2.74	-38.34	-44.31	-73.10			
BLK-C	0.03	10.02	3.99	1.47	-0.33	35.16	-12.93	212.23	263.74			
<i>Vector Copula Model VAs:</i>												
A1: (GVC-F5 & M1)	15.43	4.90	10.07	1.81	-0.55	17.84	CI	CI	CI			
A2: (GVC-F5 & M1-YJ)	19.57	15.24	19.33	8.63	-0.61	56.13	CI	CI	CI			
A3: (GVC-I & M1)	25.57	10.50	25.96	4.77	-0.31	47.72	51.00	409.67	1229.27			
A4: (GVC-I & M1-YJ)	36.98	21.09	42.11	10.26	-0.27	87.93	185.63	753.43	1929.11			
A5: (GVC-I & M2)	25.35	10.29	23.86	4.94	-0.49	45.89	19.34	362.90	1172.71			
A6: (GVC-I & M2-YJ)	18.85	20.05	40.80	10.55	-1.75	85.45	121.51	700.10	1857.95			

Note: ELBO values are reported for GMF, and the differences from these values are reported for the other VAs. Higher values correspond to higher accuracy, and the bold value in each column indicates the highest ELBO value for the dataset. "CI" represents computationally infeasible using our Python code. Detailed descriptions of the different VAs are provided in the text.

$p = 5$ or 20 factors) benchmark VAs are less accurate than the proposed vector copula models for most datasets. Third, allowing for skewed univariate marginals by learning the YJ transformation parameters (as in GC-F p , BLK-C, A2, A4 and A6) increases accuracy in almost all cases. Fourth, the vector copula models A4 and A6 are the most accurate VAs for all datasets, except *cancer*. Fifth—and an important finding of this study—is that accounting for dependence between blocks improves accuracy. This can be seen with A5/A6 dominating BLK/BLK-C, which are benchmark VAs with the same multivariate marginals but where the three blocks are independent.

Figure 1 shows why GVC-I performs well. Panels (a,c) plot the posterior Spearman correlation matrices of $(\boldsymbol{\alpha}^\top, \tilde{\boldsymbol{\delta}}^\top)$ computed exactly using MCMC for *krkp* and *spam*. The main feature is that the pairs $(\alpha_i, \tilde{\delta}_j)$ exhibit high correlation when $i = j$ (but not when $i \neq j$), which is common when using global-local shrinkage priors. This feature is captured parsimoniously by Λ in GVC-I. Panels (c,d) plot the exact posterior pairwise correlations of pairs $(\alpha_i, \tilde{\delta}_i)$ against their variational estimates for GC-F5 and A4. A low rank VA, such as GC-F5, cannot approximate these values well, whereas A4 is much better in doing so. Ignoring them (as in GMF, BLK and BLK-C) also reduces accuracy.

The proposed vector copula model VAs can also be fast to calibrate. Table A1 in Part D of the Online Appendix provides computation times of the SGD algorithm implemented in Python. The VAs A3/A4 are almost as fast as GMF, while A5/A6 are only slightly slower than BLK/BLK-C which share the same marginals. The VAs A1/A2 are slow as d increases (becoming infeasible for $d = 10,000$ in the simulated datasets). This is because a fast implementation of the $O(pd^2)$ update of the Cholesky factor A in Section 3.1.1 was unavailable in Python, and we employed full $O(d^3)$ evaluation instead. Figure 2 plots ELBO values for A4 and GC-F5 against (a) SGD step, (b) wall clock time. Not only is A4 much faster per step, it converges in fewer steps to a higher value.

In a final comment, $\tilde{\xi}$ is treated as independent in the vector copula model VAs. We have also experimented with a nested $M = 3$ vector copula, where the GVC-I for $(\boldsymbol{\alpha}, \tilde{\boldsymbol{\delta}})$ is the marginal of a bivariate KVC-G that also includes $\tilde{\xi}$. This nested vector copula was slightly more accurate than A4 for most datasets; see Part E of the Online Appendix for further details.

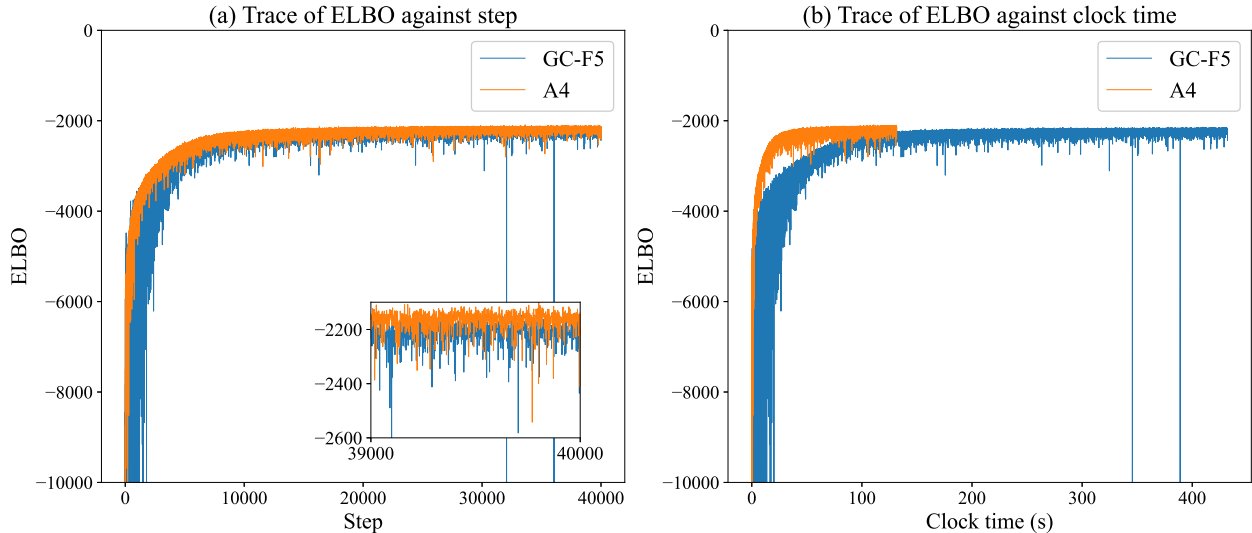


Figure 2: Plot of the ELBO values for the dataset *qsar* ($n = 8992, m = 1024$) for GC-F5 (blue line) and A4 (orange line) against (a) SGD step number, (b) wall clock time.

4.2 Example 2: Correlation matrix with LASSO regularization

The second application of VCVI is to estimate a regularized correlation matrix of a Gaussian copula model.⁴ We use this model to estimate inter-state dependence in annual changes in wealth inequality (measured by the GINI coefficient) for r U.S. states using panel data from 1916 to 2018 provided by Mark Frank on his website www.shsu.edu/eco_mvuf/inequality.html. For each state, the observations are transformed using nonparametric marginals followed by the standard normal quantile function. The $(r \times r)$ correlation matrix Σ of these transformed data is the parameter of the Gaussian copula. Pinheiro and Bates (1996) show that the lower triangular Cholesky factor of Σ can be uniquely parameterized by angles $\tilde{\beta} = (\tilde{\beta}_1, \dots, \tilde{\beta}_{r(r-1)/2})^\top$. Each angle $\tilde{\beta}_i \in [0, \pi)$ is transformed to the real line by setting $\beta_i = \Phi^{-1}(\tilde{\beta}_i/\pi)$; see Smith and Loaiza-Maya (2023) for a detailed description of this parameterization and example.

Regularization is useful because there are only $n = 103$ observations to estimate the $r(r-1)/2$ parameters. To illustrate the flexibility of our VCVI method we employ the Bayesian LASSO

⁴This copula model is for the observed data, and is not to be confused with the vector and conventional copula models that are used as VAs of the posterior distribution.

of [Figueiredo \(2003\)](#). This is a global-local shrinkage prior where

$$\beta_i|\delta_i \sim \mathcal{N}(0, \delta_i) \quad \text{and} \quad \delta_i|g \sim \text{Exp}(g/2),$$

with $\text{Exp}(\kappa)$ denoting an exponential distribution with rate κ . It can be shown that a partial correlation is zero iff $\beta_i = 0$ ([Lewandowski et al., 2009](#)) so that shrinking β_i towards zero is equivalent to shrinking these partial correlations towards zero too. To simplify the geometry of the posterior, a non-centered parameterization for β_i is used, such that $\beta_i = \alpha_i\sqrt{\delta_i}$ with $\alpha_i \sim N(0, 1)$ and $\sqrt{g} \sim \text{Exp}(1)$. Let $\tilde{\delta}_i = \log(\delta_i)$, $\tilde{g} = \log(g)$, $\boldsymbol{\alpha} = (\alpha_1, \dots, \alpha_{r(r-1)/2})^\top$ and $\tilde{\boldsymbol{\delta}} = (\tilde{\delta}_1, \dots, \tilde{\delta}_{r(r-1)/2})^\top$, then $\boldsymbol{\theta} = (\boldsymbol{\alpha}^\top, \tilde{\boldsymbol{\delta}}^\top, \tilde{g})^\top$.

The same VAs and blocking strategies are adopted as with the previous example because the between dependence structures in $\boldsymbol{\theta}$ are similar. There are 49 U.S. states in our data (Alaska and Hawaii are omitted due to missing data, and DC is included as a state), which we order by population and compute inference for Σ when $r = 5, 10, 20, 30, 49$ states (so that there five datasets). The accuracy of the VAs are summarized in [Table 3](#). The same five observations made in the previous example apply equally here to this different statistical model and global-local shrinkage prior.

In addition, we found that SGD was slow to converge for G-Fp and CG-Fp models, whereas the vector copula models were fast. To illustrate, [Figure 3](#) show the performance of VAs GC-F5 and A4 on the $r = 10$ state dataset. Panel (a) shows that the A4 was not only the most accurate VA, but that the SGD algorithm obtained its optimum within a few thousands steps, whereas it took 20,000 steps for GC-F5. For the case of $r = 49$ states, G-F5 and GC-F5 did not converge in 200,000 steps. When $r = 10$ it is possible to compute the exact posterior using (slow) MCMC. [Figure 3\(b\)](#) plots the true posterior mean of $\boldsymbol{\beta}$ against the variational posterior means for the two VAs, further demonstrating the increased accuracy of the VCVI method.

4.3 Example 3: Unobserved Component Stochastic Volatility Model

[Chan \(2017\)](#) notes that a successful univariate model for inflation is a stochastic volatility model

Table 3: ELBO values for different VAs for the regularized correlation matrix Σ

Number of U.S. States	$r = 5$	$r = 10$	$r = 20$	$r = 30$	$r = 49$
Dimension of θ	21	91	381	871	2353
<i>Benchmark VAs:</i>					
GMF	-553.93	-1039.24	-2038.91	-3152.38	-5548.02
G-F5	5.55	6.14	4.52	2.87	DNC
GC-F5	6.39	9.33	12.29	20.99	DNC
BLK	0.21	3.16	1.03	0.14	-1.36
BLK-C	0.66	5.72	13.14	32.76	89.94
<i>Vector Copula Model VAs:</i>					
A1: (GVC-F5 & M1)	5.94	8.61	6.42	6.83	5.16
A2: (GVC-F5 & M1-YJ)	8.01	11.97	19.05	39.09	97.66
A3: (GVC-I & M1)	8.51	28.54	53.26	75.52	94.91
A4: (GVC-I & M1-YJ)	10.91	35.48	71.07	109.90	181.98
A5: (GVC-I & M2)	8.59	28.61	53.25	75.47	94.29
A6: (GVC-I & M2-YJ)	10.64	34.96	70.96	110.06	181.25

Note: The posterior is for the $(r \times r)$ regularized correlation matrix Σ of the Gaussian copula model for U.S. wealth inequality panel data. The columns give results for $r = 5, 10, 20, 30$ and 49 U.S. states, and the VAs (rows) are described in Section 4.2. ELBO values are reported for GMF, and the differences from these values are reported for the other VAs. Higher values correspond to greater accuracy, with the largest value in each column in bold. DNC denotes ‘‘Did Not Converge’’ within 200,000 iterations.

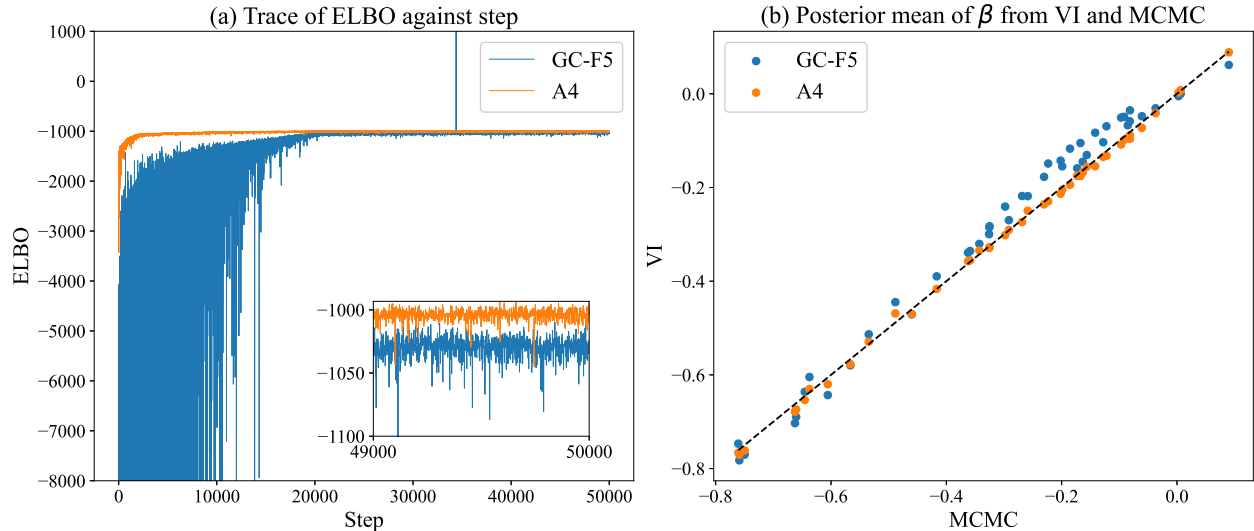


Figure 3: Comparison of two approximations GC-F5 (blue) and A4 (orange) for the regularized correlation matrix example with $r = 10$. Panel (a) plots the ELBO values against SGD step. Panel (b) plot the exact posterior mean of β computed using MCMC (horizontal axis) against the variational posterior means (vertical axis). Greater alignment on the 45 degree line corresponds to higher accuracy.

Table 4: Size, speed and accuracy of VAs in the UCSV example

	# of Variational Parameters	Time (s) Per 1000 Steps	ELBO
<i>Benchmark VAs:</i>			
GMF	1144	0.17	-95.26
GC-F5	4566	1.48	-92.85
GC-F20	12966	1.60	-97.70
BLK-C	2295	3.04	-59.75
<i>Vector Copula Model VAs:</i>			
GVC-F5	5146	10.01	-58.91
GVC-F20	13546	10.08	-57.79
GVC-I	2578	3.01	-58.90
KVC-G	2301	3.60	-59.71

Note: The approximations BLK-C, GVC-F p , GVC-I and KVC-G all have the same M1 marginals with band one L_j^{-1} matrices for $\boldsymbol{\mu}$ and $\boldsymbol{\zeta}$ and unconstrained lower triangular matrix L_3 for $\boldsymbol{\theta}_3$. The number of variational parameters is $|\boldsymbol{\lambda}|$. Times are reported for implementation in Python on an Apple M3 Max laptop. Higher ELBO values indicate greater accuracy, with the largest value in bold.

with an unobserved component (UCSV). We apply this to $T = 282$ quarterly U.S. inflation observations $y_t = \log(P_t) - \log(P_{t-1})$, where P_t is the seasonally-adjusted GDP price deflator from 1954Q1 to 2024Q3.⁵ The UCSV model decomposes $y_t = \mu_t + e^{\zeta_t/2}\varepsilon_t$, with disturbance $\varepsilon_t \sim \mathcal{N}(0, 1)$ and first order autoregressive processes in the mean and logarithmic volatility

$$\mu_t | \mu_{t-1}, \bar{\mu}, \rho_\mu, \sigma_\mu \sim \mathcal{N}(\bar{\mu} + \rho_\mu(\mu_{t-1} - \bar{\mu}), \sigma_\mu^2),$$

$$\zeta_t | \zeta_{t-1}, \bar{\zeta}, \rho_\zeta, \sigma_\zeta \sim \mathcal{N}(\bar{\zeta} + \rho_\zeta(\zeta_{t-1} - \bar{\zeta}), \sigma_\zeta^2),$$

with $\mu_0 \sim \mathcal{N}(\bar{\mu}, \sigma_\mu^2/(1-\rho_\mu^2))$ and $\zeta_0 \sim \mathcal{N}(\bar{\zeta}, \sigma_\zeta^2/(1-\rho_\zeta^2))$. As is common for this model, proper priors are adopted that bound $0 < \rho_\mu < 0.985$ and $0 < \rho_\zeta < 0.985$, so that the mean and log-volatility processes are stationary, numerically stable and have positive serial dependence.⁶

This model is readily estimated using MCMC (Chan, 2017) so that the accuracy of the variational estimates can be judged. The parameter vector is $\boldsymbol{\theta} = (\boldsymbol{\mu}^\top, \boldsymbol{\zeta}^\top, \boldsymbol{\theta}_3^\top)^\top$, where $\boldsymbol{\mu} = (\mu_1, \dots, \mu_T)^\top$, $\boldsymbol{\zeta} = (\zeta_1, \dots, \zeta_T)^\top$, $\boldsymbol{\theta}_3 = (\bar{\mu}, \tilde{\rho}_\mu, \tilde{\sigma}_\mu^2, \bar{\zeta}, \tilde{\rho}_\zeta, \tilde{\sigma}_\zeta^2)$ with $\tilde{\rho}_l = \log\left(\frac{\rho_l/0.985}{1-\rho_l/0.985}\right)$, $\tilde{\sigma}_l^2 = \log(\sigma_l^2)$ for $l \in \{\mu, \zeta\}$

⁵The implicit price deflator series [GDPDEF], was retrieved from the Federal Reserve Bank of St. Louis; <https://fred.stlouisfed.org/series/GDPDEF>, January 16, 2025.

⁶The priors are $\bar{\mu} \sim \mathcal{N}(0.5, 1000)$, $\rho_\mu \sim \mathcal{N}(0.9, 0.04)$ with $0 < \rho_\mu < 0.985$, $\sigma_\mu^2 \sim \mathcal{IG}(2, 0.001)$, $\bar{\zeta} \sim \mathcal{N}(-2, 1000)$, $\rho_\zeta \sim \mathcal{N}(0.9, 0.04)$ with $0 < \rho_\zeta < 0.985$ and $\sigma_\zeta^2 \sim \mathcal{IG}(2, 0.001)$.

transformed to be unconstrained on the real line. An important feature of the posterior is that the processes $\{\mu_t\}$ and $\{\zeta_t\}$ exhibit strong and varying near Markov positive serial dependence. Partitioning θ into the three blocks μ , ζ and θ_3 allows tailoring of the marginal posteriors to capture this. For both μ and ζ we adopt marginals M1 with L_j^{-1} a band 1 lower triangular matrix. For example, when the YJ parameters $\eta = (1, \dots, 1)$, M1 is Gaussian with band one precision matrix $S_j^{-1} L_j^{-\top} L_j^{-1} S_j^{-1}$. For θ_3 we also use marginal M1, but with matrix L_3 having unconstrained lower triangular elements. We use VAs with 3-block GVC-F p and KVC vector copulas to link these three marginals, as well as an independent block posterior (BLK-C) with the same M1 marginals for comparison. Additionally, we use GVC-I to capture the contemporaneous dependence between μ_t and ζ_t with an independent block θ_3 . The posterior is also approximated by GMF and GC-F5 as benchmark VAs.

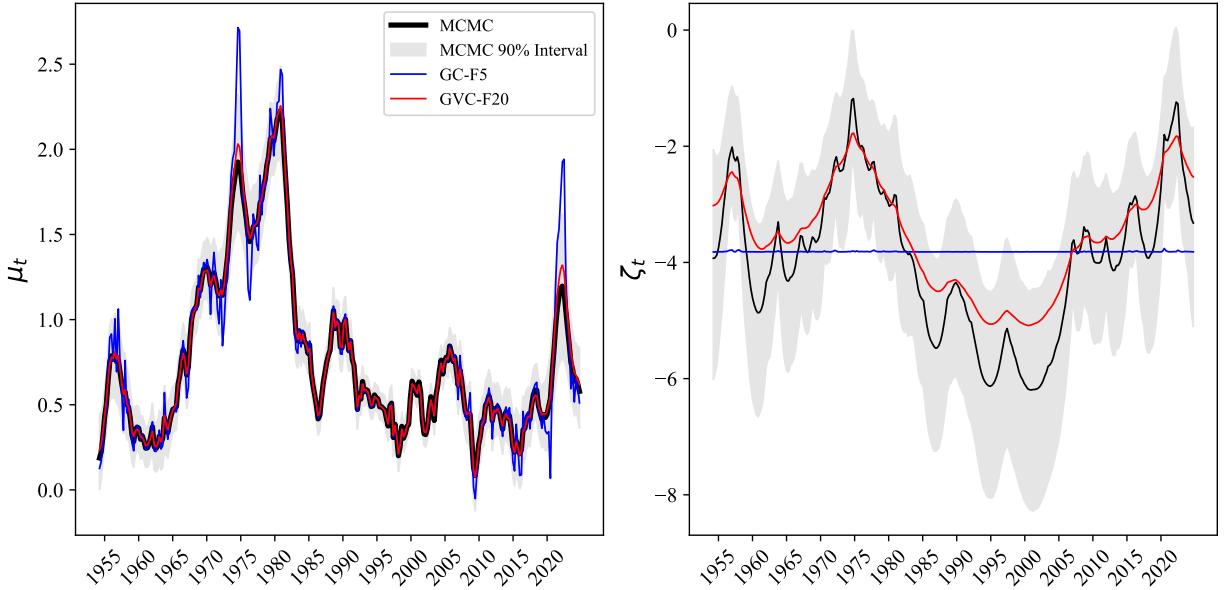


Figure 4: Comparison of the μ and ζ from the UCSV U.S. inflation example. Posterior means from different methods are plotted in solid lines. These are provided for the VAs GC-F5 (blue) and GVC-F20 (red), along with the exact posterior computed using MCMC (black). The shaded area represents the 90% interval derived from the MCMC draws.

The size, speed and accuracy of the different VAs are reported in Table 4. Using the marginals M1 with band one L_j^{-1} for μ and ζ greatly increases the accuracy of the VA. In contrast, GC-F p (a Gaussian copula with a p factor dependence structure for the entire θ vector) is only slightly

more accurate than GMF. For this example, using the vector copulas to link the blocks improves the accuracy compared to BLK-C, although not as much as in the two previous examples. Figure 4 plots the posterior means of $\boldsymbol{\mu}$ and $\boldsymbol{\zeta}$ when computed exactly using MCMC and approximately using GC-F5 and GVC-F20. GVC-F20 provides an accurate estimate of $\boldsymbol{\mu}$ and an estimate of $\boldsymbol{\zeta}$ that falls within the 90% posterior probability interval (computed using MCMC). In contrast, CG-F5 gives poor estimates of $\boldsymbol{\mu}$ and $\boldsymbol{\zeta}$.

4.4 Example 4: Additive Robust Spline Smoothing

The fourth application revisits the P-spline regression model in Ong et al. (2018), but extended to the additive model

$$y_i = \alpha + \sum_{l=1}^3 g_l(x_{l,i}) + e_i. \quad (15)$$

To robustify the function estimates to outliers, the errors follow a mixture of two normals with $p(e_i) = 0.95\phi(e_i; 0, \sigma^2) + 0.05\phi(e_i; 0, 100\sigma^2)$. Each unknown function is modeled as a P-spline where $g_l(x) = \mathbf{b}_l(x)^\top \boldsymbol{\beta}_l$, with $\mathbf{b}_l(x)$ a vector of 27 cubic B-spline basis terms evaluated at x . To produce smooth function estimates, the coefficients have proper priors $\boldsymbol{\beta}_l | \kappa_l^2, \psi_l \sim \mathcal{N}(\mathbf{0}, \kappa_l^2 P(\psi_l)^{-1})$ where $P(\psi_l)$ is the band one precision matrix of an AR(1) process with autoregressive parameter ψ_l . The priors $p(\psi_l) \propto \mathbb{1}(0 < \psi_l < 0.99)$, $\alpha \sim \mathcal{N}(0, 100)$, $\sigma^2 \sim \mathcal{IG}(0.01, 0.01)$, and κ_l^2 is Weibull with shape 0.5 and scale 0.003. For VI the model parameters are transformed to the real line by setting $\tilde{\sigma}^2 = \log(\sigma^2)$, $\tilde{\kappa}_l^2 = \log(\kappa_l^2)$, and $\tilde{\psi} = \log\left(\frac{\psi_l/0.99}{1-\psi_l/0.99}\right)$.

A total of $n = 1000$ observations are generated from (15) using the three test functions $g_1(x) = \sin(4\pi x)$, $g_2(x) = 2x - 1$ and $g_3(x) = 0.25\phi(x; 0.15, 0.05^2) + 0.25\phi(x; 0.6, 0.2^2)$, $\alpha = 2$ and $\sigma = 0.1$. The vector $\mathbf{x}_i = (x_{1,i}, x_{2,i}, x_{3,i})^\top \in [0, 1]^3$ is distributed as a Gaussian copula with parameter matrix

$$\begin{bmatrix} 1 & 0.6 & 0.8 \\ 0.6 & 1 & 0.95 \\ 0.8 & 0.95 & 1 \end{bmatrix}.$$

The 11-block partition $\boldsymbol{\theta} = (\boldsymbol{\beta}_1^\top, \boldsymbol{\beta}_2^\top, \boldsymbol{\beta}_3^\top, \alpha, \tilde{\kappa}_1^2, \tilde{\psi}_1, \tilde{\kappa}_2^2, \dots, \tilde{\psi}_3, \tilde{\sigma}^2)^\top$ is used for the three vector

copula VAs GVC-F5, GVC-F20 and KVC-G. Each β_j has marginal M1 with L_j^{-1} a band 2 lower triangular matrix (so that $L_j^{-\top} L_j^{-1}$ matches the banded pattern of the prior precision P_j) and M1 is used with $d_j = 1$ for the singleton blocks. As benchmark VAs we use GMF, GC-F5, GC-F20 and an independent block posterior (BLK) with the same marginals as the vector copula VAs.

The performance of different VAs is reported in Table 5. Among benchmark VAs, GC-F p and BLK are more accurate than GMF. All vector copula VAs improve on BLK, with GVC-F20 being the most accurate VA in this example. Figure 5 plots the true function, its posterior mean estimates computed exactly using MCMC and approximately using GVC-F20. The latter are very accurate approximations to the exact posterior.

Table 5: Size, speed and accuracy of VAs in the spline smoothing example

	# of Variational Parameters	Time (s) Per 1000 Steps	ELBO
<i>Benchmark VAs:</i>			
GMF	178	0.25	-305.62
GC-F5	702	1.20	-298.45
GC-F20	1857	1.22	-297.56
BLK-C	420	1.34	-297.47
<i>Vector Copula Model VAs:</i>			
GVC-F5	856	2.92	-292.47
GVC-F20	2011	2.97	-289.07
KVC-G	456	2.41	-295.65

Note: The approximations BLK-C, GVC-F p and KVC-G all have the same M1 marginals with band two L_j^{-1} matrices for β_1 , β_2 and β_3 . The number of variational parameters is $|\lambda|$. Times are reported for implementation in Python on an Apple M3 Max laptop. Higher ELBO values indicate greater accuracy, with the largest value in bold.

5 Discussion

While VI is popular, its effectiveness is largely determined by the choice of approximation to the posterior distribution. The key is to use an approximation that captures the salient features of a posterior, while also allowing for fast solution of the optimization. Tractable block posterior approximations are attractive because they allow for tailoring of the marginals. For example, [Ansari](#)

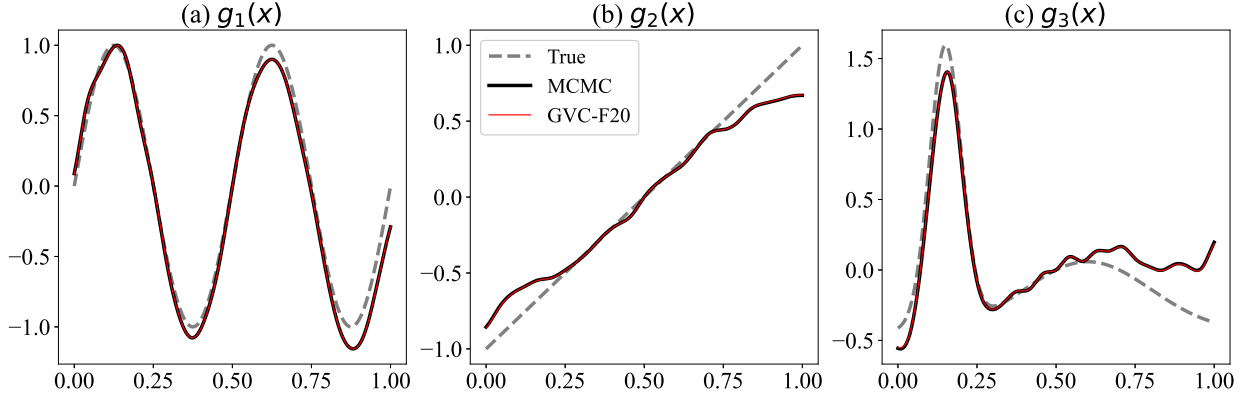


Figure 5: Posterior mean estimates of g_1 , g_2 and g_3 . The true functions (dashed line), exact posterior means computed using MCMC (black line) and variational means from GVC-F20 (red line) are plotted. The MCMC and GVC-F20 estimates are almost identical and difficult to distinguish visually. Because the functions are not unique up to an intercept in the additive model, we plot the centered functions $g_l(x) - g_l(0.5)$.

et al. (2018), Danaher et al. (2020) and Bernardi et al. (2024) do so when estimating large econometric models, and we show here that tailoring multivariate marginals is important in the UCSV and spline smoothing applications. However, it is difficult to tailor marginals while also capturing inter-block (i.e. between) dependence, so most studies—including those cited above—assume independence between the blocks. Our study is the first to suggest using vector copula models to also allow for inter-block dependence and show that this can improve the accuracy of the VAs for different posteriors.

The two multivariate marginals M1 and M2 are constructed using learnable cyclically monotone transformations that are flexible, while remaining parsimonious. They are examples of normalizing flows that are widely used as VAs in machine learning (Papamakarios et al., 2021). The GVC and KVC vector copula models were proposed by Fan and Henry (2023) for modeling low dimensional observation data. In this paper we instead use them to construct VAs in higher dimensions. For the GVC, this necessitates careful parameterization of Ω , and we suggest two approaches (i.e. GVC-F p and GVC-O/I). Both the marginals and vector copulas that we suggest have convenient generative representations that are suitable for the fast computation of efficient re-parameterized gradients. This is important when implementing SGD algorithms to solve the variational optimization.

The type of vector copula used should match the likely pattern of between dependence in the posterior. For example, when adopting a global-local shrinkage prior, such as the horseshoe in Section 4.1 or LASSO in Section 4.2, GVC-I is suitable to capture the dependence between the vectors of continuous model parameters and local hyper-parameters. This is a useful observation because global-local shrinkage priors are growing in popularity for the large Bayesian econometric models for which VI is most attractive (Korobilis et al., 2022). Other vector copulas, including GVC-Fp and KVC-G, are more suitable for capturing the between dependence in other cases. We note that KVC-G exhibits equal dependence between all elements of two blocks, which may be inappropriate for many posteriors. Nevertheless, this is not an issue when capturing the dependence between a singleton block (i.e. a block with a single scalar parameter) and other multivariate blocks. We also stress that VCVI is a highly modular framework. For example, it is possible to use a conventional copula as a multivariate marginal, as with the Gaussian copula marginals formed using M1 or M2 in our applications. It is also possible for one or more of the multivariate marginals to itself be a vector copula; something we discuss in Part E of the Online Appendix.

We conclude by noting three promising directions for future work. First, because any learnable cyclically monotone transformation can be used to define the marginals, an exploration of others (Bryan et al., 2021, Makkuva et al., 2020) that can increase accuracy at low computational cost is worthwhile. Second, the GVC can be extended to other elliptical vector copulas using generative representations for elliptical distributions, such as those discussed by Kano (1994). Additionally, the Gaussian nesting copula C_0 of the KVC can be replaced by more flexible copulas, including vine copulas (Aas et al., 2009). Finally, the VCVI method presented here has the potential to provide fast and accurate estimates of some challenging large models where mean field VAs can be poor. These include Bayesian neural networks with layer-specific horseshoe priors as in Ghosh et al. (2019), vector autoregressions with hierarchical shrinkage as in Gefang et al. (2023) and big non-nested (Goplerud, 2022) and crossed (Menictas et al., 2023) random effects models.

Appendix A Cyclically Monotone Functions M1 and M2

We show that M1 and M2 are cyclical monotone functions. Let $\mathbf{x}_j \in \mathbb{R}^{d_j}$ and $\mathbf{u}_j \in [0, 1]^{d_j}$. For M1, we have $T_j(\mathbf{u}_j) = T_{j,4} \circ T_{j,3} \circ T_{j,2} \circ T_{j,1}(\mathbf{u}_j)$ with $T_{j,4}(\mathbf{x}_j) = \mathbf{b}_j + S_j \mathbf{x}_j$, $T_{j,3}(\mathbf{x}_j) = \underline{k}_{\eta_j}(\mathbf{x}_j)$, $T_{j,2}(\mathbf{x}_j) = L_j \mathbf{x}_j$ and $T_{j,1}(\mathbf{u}_j) = \underline{\Phi}^{-1}(\mathbf{u}_j)$. It is straightforward to check that $T_{j,i}$ corresponds to the gradient of a convex function $\nabla \psi_{j,i}$, and thus $T_{j,i}$ is cyclically monotone. Specifically, we check the Hessian matrix of $\psi_{j,i}$ to be positive definite so that $\psi_{j,i}$ is a convex function. We have $\partial T_{j,4} / \partial \mathbf{x}_j = S_j$ and $\partial T_{j,2} / \partial \mathbf{x}_j = L_j$. By definition, S_j is a diagonal matrix with positive elements and L_j is a lower triangular matrix with ones on its diagonal. As a result, the Hessian matrices of $\psi_{j,4}$ and $\psi_{j,2}$ are positive definite. Additionally, $T_{j,3}$ and $T_{j,1}$ are element-wise monotonically increasing functions, and thus $\partial T_{j,3} / \partial \mathbf{x}_j$ and $\partial T_{j,1} / \partial \mathbf{u}_j$ are diagonal matrices with positive elements, which are positive definite.

For M2, we have $T_j(\mathbf{u}_j) = T_{j,3} \circ T_{j,2} \circ T_{j,1}(\mathbf{u}_j)$ with $T_{j,3}(\mathbf{x}_j) = \mathbf{b}_j + \underline{k}_{\eta_j}(\mathbf{x}_j)$, $T_{j,2}(\mathbf{x}_j) = E_j \mathbf{x}_j$ and $T_{j,1}(\mathbf{u}_j) = \underline{\Phi}^{-1}(\mathbf{u}_j)$. Similarly, $\partial T_{j,3} / \partial \mathbf{x}_j$, $\partial T_{j,2} / \partial \mathbf{x}_j$ and $\partial T_{j,1} / \partial \mathbf{u}_j$ are positive definite matrices.

Appendix B Kendall Vector Copula

Let $\mathbf{U}_j = (U_{j,1}, \dots, U_{j,d_j})^\top \in [0, 1]^{d_j}$ be a random vector. Let \mathbf{U}_j be distributed as an Archimedean copula C_j with generator function ψ_j , so that $C_j(\mathbf{U}_j) = \psi_j^{-1}(\sum_{b=1}^{d_j} \psi_j(U_{j,b}))$. [McNeil and Nešlehová \(2009\)](#) give a useful stochastic representation $\mathbf{U}_j \stackrel{d}{=} \psi_j^{-1}(R_j \mathbf{S}_j)$, where $\mathbf{S}_j = (S_1, \dots, S_{d_j})^\top$ is uniformly distributed on the d_j -dimensional simplex, and $R_j = \sum_{b=1}^{d_j} \psi_j(U_{j,b})$ has the distribution function

$$F_{R_j}(x) = 1 - \sum_{b=0}^{d_j-2} \frac{(-1)^b x^b \psi_j^{-1(b)}(x)}{b!} - \frac{(-1)^{d_j-1} x^{d_j-1} \psi_{j+}^{-1(d_j-1)}(x)}{(d_j-1)!}, x \in [0, \infty),$$

with $\psi_j^{-1(b)}$ the b -th derivative of the inverse function of ψ_j , and the function $\psi_{j+} = \max(0, \psi_j)$.

A hierarchical Kendall copula ([Brechmann, 2014](#)) nests the dependence between $\mathbf{U}_1, \dots, \mathbf{U}_M$ in a nesting copula $C_0(V_1, \dots, V_M)$, where $V_j = K_j(C_j(\mathbf{U}_j))$, and K_j is the Kendall distribution function of the random variable $C_j(\mathbf{U}_j)$. [Barbe et al. \(1996\)](#) give an expression of the Kendall

distribution function with the generator ψ_j :

$$K_j(t) = t + \sum_{b=1}^{d_j-1} \frac{(-1)^b}{b!} \psi_j(t)^b (\psi_j^{-1})^{(b)}(\psi_j(t)).$$

A KVC is a hierarchical Kendall copula with independence cluster copulas C_j , for $j = 1, \dots, M$.

An independence copula is an Archimedean copula with generator function $\psi_j(t) = -\ln(t)$, so that $\mathbf{U}_j \stackrel{d}{=} \exp(-R_j \mathbf{S}_j)$. Moreover, $\psi_{j+}^{-1}(x) = \max(0, e^{-x}) = e^{-x}$, $\psi_j^{-1(b)}(x) = \psi_{j+}^{-1(b)}(x) = (-1)^b e^{-x}$, and

$$\begin{aligned} F_{R_j}(x) &= 1 - \sum_{b=0}^{d_j-1} \frac{(-1)^b x^b \psi_j^{-1(b)}(x)}{b!} \\ &= 1 - \sum_{b=0}^{d_j-1} \frac{(-1)^b x^b (-1)^b e^{-x}}{b!} \\ &= 1 - \sum_{b=0}^{d_j-1} \frac{x^b e^{-x}}{b!}, \quad x \in [0, \infty), \end{aligned} \tag{16}$$

which is the distribution function of the Erlang distribution with the scale parameter 1 and shape parameter d_j . The Kendall distribution function of an independence copula is tractable:

$$\begin{aligned} K_j(t) &= t + \sum_{b=1}^{d_j-1} \frac{(-1)^b}{b!} (-\ln t)^b (-1)^b \exp(-(-\ln t)) \\ &= t + \sum_{b=1}^{d_j-1} \frac{t(-\ln t)^b}{b!} \\ &= \sum_{b=0}^{d_j-1} \frac{t(-\ln t)^b}{b!}. \end{aligned} \tag{17}$$

For a KVC, the random variable $V_j = K_j(C_j(\mathbf{U}_j)) = K_j(\psi_j^{-1}(\sum_{b=1}^{d_j} \psi_j(U_{j,b}))) = K_j(\psi_j^{-1}(R_j)) = K_j(\exp(-R_j))$. Using the expression at (17), we have $V_j = \sum_{b=0}^{d_j-1} \frac{R_j^b \exp(-R_j)}{b!} = 1 - F_{R_j}(R_j)$.

These derivations provide a way to sample from the KVC. First sample $\mathbf{v} = (v_1, \dots, v_M)^\top \sim C_0$, and then for $j = 1, \dots, M$ set $r_j = F_{R_j}^{-1}(1 - v_j)$, where $F_{R_j}^{-1}$ is the quantile function of the Erlang distribution as specified above. Then, for $j = 1, \dots, M$, sample the vector of independent exponentials $\mathbf{e} = (e_1, \dots, e_{d_j})^\top$ and compute $\mathbf{s}_j = (s_1, \dots, s_{d_j})^\top$ with $\mathbf{s}_j = \frac{\mathbf{e}_j}{\|\mathbf{e}_j\|}$. Finally, set $\mathbf{u}_j = \exp(-r_j \mathbf{s}_j)$, and $\mathbf{u} = (\mathbf{u}_1^\top, \dots, \mathbf{u}_M^\top)^\top$ is a draw from a KVC; see Algorithm 2.

References

- Aas, K., Czado, C., Frigessi, A., and Bakken, H. (2009). Pair-copula constructions of multiple dependence. *Insurance: Mathematics and Economics*, 44(2):182–198.
- Ansari, A., Li, Y., and Zhang, J. Z. (2018). Probabilistic topic model for hybrid recommender systems: A stochastic variational bayesian approach. *Marketing Science*, 37(6):987–1008.
- Barbe, P., Genest, C., Ghoudi, K., and Rémillard, B. (1996). On Kendall’s process. *Journal of Multivariate Analysis*, 58(2):197–229.
- Bernardi, M., Bianchi, D., and Bianco, N. (2024). Variational inference for large Bayesian vector autoregressions. *Journal of Business & Economic Statistics*, 42:1066–1082.
- Brechmann, E. C. (2014). Hierarchical kendall copulas: Properties and inference. *Canadian Journal of Statistics*, 42(1):78–108.
- Bryan, J. G., Niles-Weed, J., and Hoff, P. D. (2021). The multirank likelihood for semiparametric canonical correlation analysis. *arXiv preprint arXiv:2112.07465*.
- Carvalho, C. M., Polson, N. G., and Scott, J. G. (2010). The horseshoe estimator for sparse signals. *Biometrika*, 97(2):465–480.
- Chan, J. C. (2017). The stochastic volatility in mean model with time-varying parameters: An application to inflation modeling. *Journal of Business & Economic Statistics*, 35(1):17–28.
- Danaher, P. J., Danaher, T. S., Smith, M. S., and Loaiza-Maya, R. (2020). Advertising effectiveness for multiple retailer-brands in a multimedia and multichannel environment. *Journal of Marketing Research*, 57(3):445–467.
- Deng, L., Smith, M. S., and Maneesoonthorn, W. (2024). Large skew-t copula models and asymmetric dependence in intraday equity returns. *Journal of Business & Economic Statistics*, pages 1–17.
- Fan, Y. and Henry, M. (2023). Vector copulas. *Journal of Econometrics*, 234(1):128–150.
- Figueiredo, M. A. (2003). Adaptive sparseness for supervised learning. *IEEE Transactions on Pattern Analysis and Machine Intelligence*, 25(9):1150–1159.
- Frahm, G., Junker, M., and Szimayer, A. (2003). Elliptical copulas: applicability and limitations. *Statistics & Probability Letters*, 63(3):275–286.
- Gefang, D., Koop, G., and Poon, A. (2023). Forecasting using variational bayesian inference in large vector autoregressions with hierarchical shrinkage. *International Journal of Forecasting*, 39(1):346–363.
- Genest, C., Quesada Molina, J., and Rodríguez Lallena, J. (1995). De l’impossibilité de construire des lois à marges multidimensionnelles données à partir de copules. *Comptes rendus de l’Académie des sciences. Série 1, Mathématique*, 320(6):723–726.
- Ghosh, S., Yao, J., and Doshi-Velez, F. (2018). Structured variational learning of bayesian neural networks with horseshoe priors. In *International Conference on Machine Learning*, pages 1744–1753. PMLR.

- Ghosh, S., Yao, J., and Doshi-Velez, F. (2019). Model selection in bayesian neural networks via horseshoe priors. *Journal of Machine Learning Research*, 20(182):1–46.
- Goplerud, M. (2022). Fast and accurate estimation of non-nested binomial hierarchical models using variational inference. *Bayesian Analysis*, 17(2):623–650.
- Goplerud, M., Papaspiliopoulos, O., and Zanella, G. (2023). Partially factorized variational inference for high-dimensional mixed models. *arXiv preprint arXiv:2312.13148*.
- Gunawan, D., Kohn, R., and Nott, D. (2024). Flexible variational Bayes based on a copula of a mixture. *Journal of Computational and Graphical Statistics*, 33(2):665–680.
- Han, S., Liao, X., Dunson, D., and Carin, L. (2016). Variational gaussian copula inference. In *Artificial Intelligence and Statistics*, pages 829–838. PMLR.
- Headrick, T. C., Kowalchuk, R. K., and Sheng, Y. (2008). Parametric probability densities and distribution functions for tukey g-and-h transformations and their use for fitting data. *Applied Mathematical Sciences*, 2(9):449–462.
- Ingraham, J. and Marks, D. (2017). Variational inference for sparse and undirected models. In *International Conference on Machine Learning*, pages 1607–1616. PMLR.
- Joe, H. (2014). *Dependence modeling with copulas*. CRC press.
- Jones, M. C. and Pewsey, A. (2009). Sinh-arcsinh distributions. *Biometrika*, 96(4):761–780.
- Kano, Y. (1994). Consistency property of elliptic probability density functions. *Journal of Multivariate Analysis*, 51(1):139–147.
- Kingma, D. P. and Ba, J. (2014). Adam: A method for stochastic optimization. *arXiv preprint arXiv:1412.6980*.
- Kingma, D. P. and Welling, M. (2013). Auto-encoding variational bayes. *arXiv preprint arXiv:1312.6114*.
- Koop, G. and Korobilis, D. (2023). Bayesian dynamic variable selection in high dimensions. *International Economic Review*, 64(3):1047–1074.
- Korobilis, D., Shimizu, K., et al. (2022). Bayesian approaches to shrinkage and sparse estimation. *Foundations and Trends® in Econometrics*, 11(4):230–354.
- Lang, S. and Brezger, A. (2004). Bayesian p-splines. *Journal of Computational and Graphical Statistics*, 13(1):183–212.
- Lewandowski, D., Kurowicka, D., and Joe, H. (2009). Generating random correlation matrices based on vines and extended onion method. *Journal of Multivariate Analysis*, 100(9):1989–2001.
- Loaiza-Maya, R. and Nibbering, D. (2023). Fast variational bayes methods for multinomial probit models. *Journal of Business & Economic Statistics*, 41(4):1352–1363.
- Makkuva, A., Taghvaei, A., Oh, S., and Lee, J. (2020). Optimal transport mapping via input convex neural networks. In *International Conference on Machine Learning*, pages 6672–6681. PMLR.

- McNeil, A. J. and Nešlehová, J. (2009). Multivariate archimedean copulas, d -monotone functions and ℓ_1 -norm symmetric distributions. *The Annals of Statistics*, 37(5B):3059–3097.
- Menictas, M., Di Credico, G., and Wand, M. P. (2023). Streamlined variational inference for linear mixed models with crossed random effects. *Journal of Computational and Graphical Statistics*, 32(1):99–115.
- Nelsen, R. B. (2006). *An Introduction to Copulas*. Springer-Verlag, New York, Secaucus, NJ, USA.
- Ong, V. M.-H., Nott, D. J., and Smith, M. S. (2018). Gaussian variational approximation with a factor covariance structure. *Journal of Computational and Graphical Statistics*, 27(3):465–478.
- Ormerod, J. T. and Wand, M. P. (2010). Explaining variational approximations. *The American Statistician*, 64(2):140–153.
- Papamakarios, G., Nalisnick, E., Rezende, D. J., Mohamed, S., and Lakshminarayanan, B. (2021). Normalizing flows for probabilistic modeling and inference. *The Journal of Machine Learning Research*, 22(1):2617–2680.
- Petersen, K. B., Pedersen, M. S., et al. (2008). The matrix cookbook. *Technical University of Denmark*, 7(15):510.
- Pinheiro, J. C. and Bates, D. M. (1996). Unconstrained parametrizations for variance-covariance matrices. *Statistics and Computing*, 6:289–296.
- Quiroz, M., Nott, D. J., and Kohn, R. (2023). Gaussian variational approximations for high-dimensional state space models. *Bayesian Analysis*, 18(3):989–1016.
- Ren, H., Zhao, S., and Ermon, S. (2019). Adaptive antithetic sampling for variance reduction. In *International Conference on Machine Learning*, pages 5420–5428. PMLR.
- Ressel, P. (2019). Copulas, stable tail dependence functions, and multivariate monotonicity. *Dependence Modeling*, 7(1):247–258.
- Rezende, D. J., Mohamed, S., and Wierstra, D. (2014). Stochastic backpropagation and approximate inference in deep generative models. In *International Conference on Machine Learning*, pages 1278–1286. PMLR.
- Salimans, T. and Knowles, D. A. (2013). Fixed-form variational posterior approximation through stochastic linear regression. *Bayesian Analysis*, 8(4):837 – 882.
- Salomone, R., Yu, X., Nott, D. J., and Kohn, R. (2023). Structured variational approximations with skew normal decomposable graphical models. *arXiv preprint arXiv:2302.03348*.
- Smith, M. S. and Loaiza-Maya, R. (2023). Implicit copula variational inference. *Journal of Computational and Graphical Statistics*, 32(3):769–781.
- Smith, M. S., Loaiza-Maya, R., and Nott, D. J. (2020). High-dimensional copula variational approximation through transformation. *Journal of Computational and Graphical Statistics*, 29(4):729–743.
- Tan, L. S. and Nott, D. J. (2018). Gaussian variational approximation with sparse precision matrices. *Statistics and Computing*, 28:259–275.

- Titsias, M. and Lázaro-Gredilla, M. (2014). Doubly stochastic variational bayes for non-conjugate inference. In *International Conference on Machine Learning*, pages 1971–1979. PMLR.
- Tran, D., Blei, D., and Airoldi, E. M. (2015). Copula variational inference. *Advances in Neural Information Processing Systems*, 28.
- Virtanen, P., Gommers, R., Oliphant, T. E., Haberland, M., Reddy, T., Cournapeau, D., Burovski, E., Peterson, P., Weckesser, W., Bright, J., van der Walt, S. J., Brett, M., Wilson, J., Millman, K. J., Mayorov, N., Nelson, A. R. J., Jones, E., Kern, R., Larson, E., Carey, C. J., Polat, İ., Feng, Y., Moore, E. W., VanderPlas, J., Laxalde, D., Perktold, J., Cimrman, R., Henriksen, I., Quintero, E. A., Harris, C. R., Archibald, A. M., Ribeiro, A. H., Pedregosa, F., van Mulbregt, P., and SciPy 1.0 Contributors (2020). SciPy 1.0: Fundamental Algorithms for Scientific Computing in Python. *Nature Methods*, 17:261–272.
- Xu, M., Quiroz, M., Kohn, R., and Sisson, S. A. (2019). Variance reduction properties of the reparameterization trick. In *The 22nd International Conference on Artificial Intelligence and Statistics*, pages 2711–2721. PMLR.
- Yeo, I.-K. and Johnson, R. A. (2000). A new family of power transformations to improve normality or symmetry. *Biometrika*, 87(4):954–959.
- Zeiler, M. D. (2012). Adadelta: an adaptive learning rate method. *arXiv preprint arXiv:1212.5701*.

Online Appendix for “Vector Copula Variational Inference and Dependent Block Posterior Approximations”

This Online Appendix has five parts:

Part A: Notational conventions and matrix differentiation rules used

Part B: Details of GVC-O

B.1: Inverse of Ω

B.2: Analytical gradients of A3 (GVC-I & M1)

Part C: Efficient re-parameterized gradients for VCVI and KVC-G

C.1: VCVI

C.2: KVC-G

Part D: Additional empirical information

Part E: Nested vector copula density

E.1: Re-parameterization trick

E.2: Empirical results

Part A: Notational conventions and matrix differentiation rules used

We outline the notational conventions that we adopt in computing derivatives throughout the paper. For a d -dimensional vector valued function $g(\mathbf{x})$ of an n -dimensional argument \mathbf{x} , $\frac{\partial g}{\partial \mathbf{x}}$ is the $d \times n$ matrix with element (i, j) $\frac{\partial g_i}{\partial x_j}$. This means for a scalar $g(\mathbf{x})$, $\frac{\partial g}{\partial \mathbf{x}}$ is a row vector. When discussing the gradients we also sometimes write $\nabla_x g(\mathbf{x}) = \left[\frac{\partial g}{\partial \mathbf{x}} \right]^\top$, which is a column vector. When the function $g(\mathbf{x})$ or the argument \mathbf{x} are matrix valued, then $\frac{\partial g}{\partial \mathbf{x}}$ is taken to mean $\frac{\partial \text{vec}(g(\mathbf{x}))}{\partial \text{vec}(\mathbf{x})}$, where $\text{vec}(A)$ denotes the vectorization of a matrix A obtained by stacking its columns one underneath another.

When an arithmetic operator is applied to a vector, such as subtraction, exponential and the square root, it is applied to each element in that vector.

Part B: Details of GVC-O

B.1: Inverse of Ω

We use the block matrix inverse formula:

$$\begin{bmatrix} A & B \\ C & D \end{bmatrix}^{-1} = \begin{bmatrix} A^{-1} + A^{-1}B(D - CA^{-1}B)^{-1}CA^{-1} & -A^{-1}B(D - CA^{-1}B)^{-1} \\ -(D - CA^{-1}B)^{-1}CA^{-1} & (D - CA^{-1}B)^{-1} \end{bmatrix}$$

for the matrix

$$\Omega = \begin{bmatrix} I_{d_1} & Q_1\Lambda Q_2^\top \\ Q_2\Lambda Q_1^\top & I_{d_2} \end{bmatrix}.$$

Under the assumption that $d_1 \leq d_2$, we have shown that $(D - CA^{-1}B)^{-1} = (\Omega_2/I_{d_1})^{-1} = Q_2(I_{\tilde{d}} - \Lambda^2)^{-1}Q_2^\top$. As a result, we have

$$\begin{aligned} & A^{-1} + A^{-1}B(D - CA^{-1}B)^{-1}CA^{-1} \\ &= I_{d_1} + Q_1\Lambda Q_2^\top Q_2(I_{\tilde{d}} - \Lambda^2)^{-1}Q_2^\top Q_2\Lambda Q_1^\top \\ &= I_{d_1} + Q_1\Lambda(I_{\tilde{d}} - \Lambda^2)^{-1}\Lambda Q_1^\top \end{aligned}$$

and

$$\begin{aligned} & -A^{-1}B(D - CA^{-1}B)^{-1} \\ &= -Q_1\Lambda Q_2^\top Q_2(I_{\tilde{d}} - \Lambda^2)^{-1}Q_2^\top \\ &= -Q_1\Lambda(I_{\tilde{d}} - \Lambda^2)^{-1}Q_2^\top. \end{aligned}$$

Thus,

$$\Omega^{-1} = \begin{bmatrix} I_{d_1} + Q_1\Lambda(I_{\tilde{d}} - \Lambda^2)^{-1}\Lambda Q_1^\top & -Q_1\Lambda(I_{\tilde{d}} - \Lambda^2)^{-1}Q_2^\top \\ -Q_2(I_{\tilde{d}} - \Lambda^2)^{-1}\Lambda Q_1^\top & Q_2(I_{\tilde{d}} - \Lambda^2)^{-1}Q_2^\top \end{bmatrix}.$$

When $d_1 = d_2 = \tilde{d}$ and $Q_1 = Q_2 = I_{\tilde{d}}$,

$$\Omega = \begin{bmatrix} I_{\tilde{d}} & \Lambda \\ \Lambda & I_{\tilde{d}} \end{bmatrix}$$

and

$$\Omega^{-1} = \begin{bmatrix} I_{d_1} + \Lambda(I_{\tilde{d}} - \Lambda^2)^{-1}\Lambda & \Lambda(I_{\tilde{d}} - \Lambda^2)^{-1} \\ -(I_{\tilde{d}} - \Lambda^2)^{-1}\Lambda & (I_{\tilde{d}} - \Lambda^2)^{-1} \end{bmatrix}.$$

B.2: Analytical gradients of A3 (GVC-I & M1)

To implement this method, we first sample $\mathbf{z} = (\mathbf{z}_1^\top, \mathbf{z}_2^\top, z_3)^\top$ from $\mathcal{N}(\mathbf{0}_{m+m+1}, \tilde{\Omega})$. Here,

$$\tilde{\Omega} = \begin{bmatrix} I_m & \Lambda & \mathbf{0}_{m \times 1} \\ \Lambda & I_m & \mathbf{0}_{m \times 1} \\ \mathbf{0}_{1 \times m} & \mathbf{0}_{1 \times m} & 1 \end{bmatrix},$$

and \mathbf{z} can be sampled by the re-parameterization trick

$$\mathbf{z} = \begin{bmatrix} I_m & \mathbf{0}_{m \times m} & \mathbf{0}_{m \times 1} \\ \Lambda & \sqrt{I_m - \Lambda^2} & \mathbf{0}_{m \times 1} \\ \mathbf{0}_{1 \times m} & \mathbf{0}_{1 \times m} & 1 \end{bmatrix} \boldsymbol{\epsilon} = \begin{bmatrix} \boldsymbol{\epsilon}_1 \\ \mathbf{l} \circ \boldsymbol{\epsilon}_1 + \sqrt{\mathbf{1}_m - \mathbf{l}^2} \circ \boldsymbol{\epsilon}_2 \\ \boldsymbol{\epsilon}_3 \end{bmatrix},$$

where $\boldsymbol{\epsilon} = (\boldsymbol{\epsilon}_1^\top, \boldsymbol{\epsilon}_2^\top, \boldsymbol{\epsilon}_3^\top)^\top \sim \mathcal{N}(0, I_{m+m+1})$ and the diagonal elements of Λ is represented by the vector \mathbf{l} which has constrained values from -1 to 1.

Then $(\mathbf{u}_1^\top, \mathbf{u}_2^\top)^\top = \Phi((\mathbf{z}_1^\top, \mathbf{z}_2^\top)^\top; I_{2m})$ follows a GVC-I, and $u_3 = \Phi(z_3; I_1)$ is independent of $(\mathbf{u}_1^\top, \mathbf{u}_2^\top)^\top$. The multivariate margins are constructed by $\boldsymbol{\theta}_i = \mathbf{b}_i + S_i \Phi_i^{-1}(\mathbf{u}_i) = \mathbf{b}_i + S_i \mathbf{z}_i$ for $i = 1, 2, 3$. Thus, we note that $\boldsymbol{\theta}$ can be simply represented by $\boldsymbol{\theta} = \mathbf{b} + \mathbf{s} \circ \mathbf{z}$, where $\mathbf{b} = (\mathbf{b}_1^\top, \mathbf{b}_2^\top, b_3)^\top$, \mathbf{s} is the leading diagonal of the diagonal matrix S and \circ is the Hadamard product.

The vectors \mathbf{s} and \mathbf{l} have constrained values. We use $\mathbf{s} = \tilde{\mathbf{s}}^2$ and $\mathbf{l} = \frac{2}{\exp(-\tilde{\mathbf{l}})+1} - 1$ such that $\tilde{\mathbf{s}}$ and $\tilde{\mathbf{l}}$ are two vectors defined on the real line. As the result, the variational parameters are $\boldsymbol{\lambda} = (\tilde{\mathbf{l}}^\top, \tilde{\mathbf{s}}^\top, \mathbf{b}^\top)^\top$.

We are interested in the re-parameterized gradients:

$$\nabla_{\boldsymbol{\lambda}} \mathcal{L}(\boldsymbol{\lambda}) = \mathbb{E}_{f_{\boldsymbol{\epsilon}}} \left\{ \left[\frac{d\boldsymbol{\theta}}{d\boldsymbol{\lambda}} \right]^\top \nabla_{\boldsymbol{\theta}} (\log h(\boldsymbol{\theta}) - \log q(\boldsymbol{\theta})) \right\}.$$

Here, we evaluate $\nabla_{\boldsymbol{\theta}} \log h(\boldsymbol{\theta})$ by automatic differentiation, and $\nabla_{\boldsymbol{\theta}} \log q(\boldsymbol{\theta}) = -S^{-1} \cdot \tilde{\Omega}^{-1} \cdot \boldsymbol{\theta}$. It is straightforward to see that

$$\begin{aligned} \frac{d\boldsymbol{\theta}}{d\mathbf{b}} &= I_{2m+1}, \\ \frac{d\boldsymbol{\theta}}{d\tilde{\mathbf{s}}} &= \text{Diag}(2\tilde{\mathbf{s}} \circ \mathbf{z}), \\ \frac{d\boldsymbol{\theta}}{d\tilde{\mathbf{l}}} &= \frac{d\boldsymbol{\theta}}{d\mathbf{z}} \frac{d\mathbf{z}}{d\mathbf{l}} \frac{d\mathbf{l}}{d\tilde{\mathbf{l}}}. \end{aligned}$$

For the last term, we have

$$\frac{d\mathbf{z}}{d\mathbf{l}} = \begin{bmatrix} \mathbf{0}_{m \times m} \\ \frac{d\mathbf{z}_2}{d\mathbf{l}} \\ \mathbf{0}_{1 \times m} \end{bmatrix},$$

where

$$\frac{d\mathbf{z}_2}{d\mathbf{l}} = \text{Diag} \left(\boldsymbol{\epsilon}_1 - \frac{\mathbf{l}}{\sqrt{\mathbf{1}_m - \mathbf{l}^2}} \circ \boldsymbol{\epsilon}_2 \right).$$

Moreover,

$$\frac{d\boldsymbol{\theta}}{d\mathbf{z}} = \text{Diag}(\tilde{\mathbf{s}}^2)$$

and

$$\frac{d\mathbf{l}}{d\tilde{\mathbf{l}}} = \text{Diag} \left\{ \frac{2 \exp(-\tilde{\mathbf{l}})}{(\exp(-\tilde{\mathbf{l}}) + 1)^2} \right\}.$$

As a result,

$$\frac{d\boldsymbol{\theta}}{d\tilde{l}} = \text{Diag}(\tilde{\mathbf{s}}^2) \cdot \begin{bmatrix} \mathbf{0}_{m \times m} \\ \boldsymbol{\epsilon}_1 - \frac{\mathbf{l}}{\sqrt{\mathbf{1}_m - \mathbf{l}^2}} \circ \boldsymbol{\epsilon}_2 \\ \mathbf{0}_{1 \times m} \end{bmatrix} \cdot \text{Diag} \left\{ \frac{2 \exp(-\tilde{l})}{(\exp(-\tilde{l}) + 1)^2} \right\}.$$

Thus,

$$\begin{aligned} \nabla_{\mathbf{b}} \mathcal{L}(\boldsymbol{\lambda}) &= \nabla_{\boldsymbol{\theta}} (\log h(\boldsymbol{\theta}) - \log q(\boldsymbol{\theta})) , \\ \nabla_{\tilde{\mathbf{s}}} \mathcal{L}(\boldsymbol{\lambda}) &= 2\tilde{\mathbf{s}} \circ \mathbf{z} \circ \nabla_{\boldsymbol{\theta}} (\log h(\boldsymbol{\theta}) - \log q(\boldsymbol{\theta})) , \end{aligned}$$

and

$$\begin{aligned} \nabla_{\tilde{\mathbf{l}}} \mathcal{L}(\boldsymbol{\lambda}) &= \left\{ \text{Diag}(\tilde{\mathbf{s}}^2) \cdot \begin{bmatrix} \mathbf{0}_{m \times m} \\ \boldsymbol{\epsilon}_1 - \frac{\mathbf{l}}{\sqrt{\mathbf{1}_m - \mathbf{l}^2}} \circ \boldsymbol{\epsilon}_2 \\ \mathbf{0}_{1 \times m} \end{bmatrix} \cdot \text{Diag} \left\{ \frac{2 \exp(-\tilde{l})}{(\exp(-\tilde{l}) + 1)^2} \right\} \right\}^\top \\ &\quad \cdot \nabla_{\boldsymbol{\theta}} (\log h(\boldsymbol{\theta}) - \log q(\boldsymbol{\theta})) \\ &= \text{Diag} \left\{ \frac{2 \exp(-\tilde{l})}{(\exp(-\tilde{l}) + 1)^2} \right\} \cdot \begin{bmatrix} \mathbf{0}_{m \times m} & \text{Diag} \left(\boldsymbol{\epsilon}_1 - \frac{\mathbf{l}}{\sqrt{\mathbf{1}_m - \mathbf{l}^2}} \circ \boldsymbol{\epsilon}_2 \right) & \mathbf{0}_{m \times 1} \end{bmatrix} \\ &\quad \cdot \text{Diag}(\tilde{\mathbf{s}}^2) \cdot \nabla_{\boldsymbol{\theta}} (\log h(\boldsymbol{\theta}) - \log q(\boldsymbol{\theta})) \\ &= \frac{2 \exp(-\tilde{l})}{(\exp(-\tilde{l}) + 1)^2} \circ \left(\boldsymbol{\epsilon}_1 - \frac{\mathbf{l}}{\sqrt{\mathbf{1}_m - \mathbf{l}^2}} \circ \boldsymbol{\epsilon}_2 \right) \circ \tilde{\mathbf{s}}_{m:2m}^2 \circ [\nabla_{\boldsymbol{\theta}} (\log h(\boldsymbol{\theta}) - \log q(\boldsymbol{\theta}))]_{m:2m} , \end{aligned} \tag{A1}$$

where $m : 2m$ denotes keeping the elements from element m to $2m$ in a vector. The last equality in (A1) can be seen by treating matrix multiplications as row operations or column operations.

To conclude, we underline that only Hadamard products between vectors are required to update the variational parameters in A3 (except for $\nabla_{\boldsymbol{\theta}} \log h(\boldsymbol{\theta})$).

Part C: Efficient re-parameterized gradients for VCVI and KVC-G

C.1: VCVI

When we use a vector copula density as the variational density, equation (1) can be written as

$$\mathcal{L}(q) = \mathbb{E}_q \left[\log h(\boldsymbol{\theta}) - \log c_v(\mathbf{u}; \boldsymbol{\lambda}_{\text{vc}}) - \sum_{j=1}^M \log q_j(\boldsymbol{\theta}_j; \boldsymbol{\lambda}_j) \right], \quad (\text{A2})$$

where c_v and q_j are the probability density functions of \mathbf{u} and $\boldsymbol{\theta}_j$, respectively. Throughout the paper, $\mathbb{E}_f[g]$ denotes the expectation of a function g with respect to random vector $\mathbf{X} \sim f$ with f the density function of \mathbf{X} . Equation (A2) can be simplified as

$$\mathcal{L}(q) = \mathbb{E}_q [\log h(\boldsymbol{\theta})] - \mathbb{E}_{c_v} [\log c_v(\mathbf{u}; \boldsymbol{\lambda}_{\text{vc}})] - \sum_{j=1}^M \mathbb{E}_{q_j} [\log q_j(\boldsymbol{\theta}_j; \boldsymbol{\lambda}_j)]. \quad (\text{A3})$$

Such a simplification from (A3) enables us to evaluate the gradient efficiently. Specifically, we have

$$\begin{aligned} \nabla_{\boldsymbol{\lambda}_j} \mathbb{E}_{q_j} [\log q_j(\boldsymbol{\theta}_j; \boldsymbol{\lambda}_j)] &= \mathbb{E}_{q_j} \left[\left(\frac{d\boldsymbol{\theta}_j}{d\boldsymbol{\lambda}_j} \right)^\top \nabla_{\boldsymbol{\theta}_j} \log q_j(\boldsymbol{\theta}_j; \boldsymbol{\lambda}_j) + \nabla_{\boldsymbol{\lambda}_j} \log q_j(\boldsymbol{\theta}_j; \boldsymbol{\lambda}_j) \right] \\ &= \mathbb{E}_{q_j} \left[\left(\frac{d\boldsymbol{\theta}_j}{d\boldsymbol{\lambda}_j} \right)^\top \nabla_{\boldsymbol{\theta}_j} \log q_j(\boldsymbol{\theta}_j; \boldsymbol{\lambda}_j) \right] \end{aligned}$$

and

$$\begin{aligned} \nabla_{\boldsymbol{\lambda}_{\text{vc}}} \mathbb{E}_{c_v} [\log c_v(\mathbf{u}; \boldsymbol{\lambda}_{\text{vc}})] &= \mathbb{E}_{c_v} \left[\left(\frac{d\mathbf{u}}{d\boldsymbol{\lambda}_{\text{vc}}} \right)^\top \nabla_{\mathbf{u}} \log c_v(\mathbf{u}; \boldsymbol{\lambda}_{\text{vc}}) + \nabla_{\boldsymbol{\lambda}_{\text{vc}}} \log c_v(\mathbf{u}; \boldsymbol{\lambda}_{\text{vc}}) \right] \\ &= \mathbb{E}_{c_v} \left[\left(\frac{d\mathbf{u}}{d\boldsymbol{\lambda}_{\text{vc}}} \right)^\top \nabla_{\mathbf{u}} \log c_v(\mathbf{u}; \boldsymbol{\lambda}_{\text{vc}}) \right] \end{aligned}$$

because of the log derivative trick.

Thus, the re-parameterized gradients of (A3) are

$$\begin{aligned} \nabla_{\boldsymbol{\lambda}_{\text{vc}}} \mathcal{L}(\boldsymbol{\lambda}) &= \mathbb{E}_{f_\epsilon} \left\{ \left[\frac{d\boldsymbol{\theta}}{d\boldsymbol{\lambda}_{\text{vc}}} \right]^\top \nabla_{\boldsymbol{\theta}} \left(\log h(\boldsymbol{\theta}) - \sum_{j=1}^M \log q_j(\boldsymbol{\theta}_j; \boldsymbol{\lambda}_j) \right) - \left[\frac{d\mathbf{u}}{d\boldsymbol{\lambda}_{\text{vc}}} \right]^\top \nabla_{\mathbf{u}} \log c_v(\mathbf{u}; \boldsymbol{\lambda}_{\text{vc}}) \right\}, \\ \nabla_{\boldsymbol{\lambda}_{\text{marg}}} \mathcal{L}(\boldsymbol{\lambda}) &= \mathbb{E}_{f_\epsilon} \left\{ \left[\frac{d\boldsymbol{\theta}}{d\boldsymbol{\lambda}_{\text{marg}}} \right]^\top \nabla_{\boldsymbol{\theta}} \left(\log h(\boldsymbol{\theta}) - \sum_{j=1}^M \log q_j(\boldsymbol{\theta}_j; \boldsymbol{\lambda}_j) \right) \right\}, \quad (\text{A4}) \end{aligned}$$

where $\boldsymbol{\theta} = g_2(g_1(\boldsymbol{\epsilon}, \boldsymbol{\lambda}_{\text{vc}}), \boldsymbol{\lambda}_{\text{marg}})$ and $\mathbf{u} = g_1(\boldsymbol{\epsilon}, \boldsymbol{\lambda}_{\text{vc}})$.

C.2: KVC-G

We can further simplify $\mathbb{E}_{f_\epsilon} [c_v(\mathbf{u}; \boldsymbol{\lambda}_{\text{vc}})]$ in the context of KVC-G, where we have $f_\epsilon = p(\boldsymbol{\epsilon}_1, \mathbf{e}) =$

$p(\boldsymbol{\epsilon}_1)p(\mathbf{e})$ with $\mathbf{e} = (\mathbf{e}_1^\top, \dots, \mathbf{e}_M^\top)^\top$. The density of a Gaussian copula is

$$c_0^{Ga}(v_1, \dots, v_M; \bar{\Omega}) = |\bar{\Omega}|^{-1/2} \exp \left\{ -\frac{1}{2} \boldsymbol{\kappa}^\top (\bar{\Omega}^{-1} - I_M) \boldsymbol{\kappa} \right\},$$

where $\boldsymbol{\kappa} = \underline{\Phi}^{-1}(\mathbf{v})$ and $\mathbf{v} = (v_1, \dots, v_M)^\top$. Let \tilde{G} be the lower triangular Cholesky factor of $\bar{\Omega}$. To sample from the Gaussian copula, we set $\mathbf{v} = \underline{\Phi}(\tilde{G}\boldsymbol{\epsilon}_1)$ with $\boldsymbol{\epsilon}_1 \sim \mathcal{N}(\mathbf{0}, I_M)$. The log density under the expectation gives:

$$\begin{aligned} & E_{p(\boldsymbol{\epsilon}_1, \mathbf{e})} [\log c_v(\mathbf{u}_1, \dots, \mathbf{u}_M)] \\ &= E_{p(\boldsymbol{\epsilon}_1, \mathbf{e})} [\log c_0^{Ga}(v_1, \dots, v_M; \bar{\Omega})] \\ &= \int_{\mathbf{e}} \int_{\boldsymbol{\epsilon}_1} \log c_0^{Ga}(v_1, \dots, v_M; \bar{\Omega}) p(\boldsymbol{\epsilon}_1) p(\mathbf{e}) d\boldsymbol{\epsilon}_1 d\mathbf{e} \\ &= \int_{\boldsymbol{\epsilon}_1} \log c_0^{Ga}(v_1, \dots, v_M; \bar{\Omega}) p(\boldsymbol{\epsilon}_1) d\boldsymbol{\epsilon}_1 \int_{\mathbf{e}} p(\mathbf{e}) d\mathbf{e} \\ &= E_{p(\boldsymbol{\epsilon}_1)} [\log c_0^{Ga}(v_1, \dots, v_M; \bar{\Omega})] \\ &= E_{p(\boldsymbol{\epsilon}_1)} \left[\log \left(|\bar{\Omega}|^{-1/2} \exp \left\{ -\frac{1}{2} (\tilde{G}\boldsymbol{\epsilon}_1)^\top (\bar{\Omega}^{-1} - I_M) \tilde{G}\boldsymbol{\epsilon}_1 \right\} \right) \right] \\ &= E_{p(\boldsymbol{\epsilon}_1)} \left[-\frac{1}{2} \log |\tilde{G}\tilde{G}^\top| - \frac{1}{2} (\tilde{G}\boldsymbol{\epsilon}_1)^\top (\tilde{G}\tilde{G}^\top)^{-1} \tilde{G}\boldsymbol{\epsilon}_1 + \frac{1}{2} (\tilde{G}\boldsymbol{\epsilon}_1)^\top \tilde{G}\boldsymbol{\epsilon}_1 \right] \\ &= E_{p(\boldsymbol{\epsilon}_1)} \left[-\frac{1}{2} \log |\tilde{G}\tilde{G}^\top| - \frac{1}{2} \boldsymbol{\epsilon}_1^\top \tilde{G}^\top (\tilde{G}^\top)^{-1} \tilde{G}^{-1} \tilde{G}\boldsymbol{\epsilon}_1 + \frac{1}{2} \boldsymbol{\epsilon}_1^\top \tilde{G}^\top \tilde{G}\boldsymbol{\epsilon}_1 \right] \\ &= E_{p(\boldsymbol{\epsilon}_1)} \left[-\frac{1}{2} \log |\tilde{G}\tilde{G}^\top| - \frac{1}{2} \boldsymbol{\epsilon}_1^\top \boldsymbol{\epsilon}_1 + \frac{1}{2} \boldsymbol{\epsilon}_1^\top \tilde{G}^\top \tilde{G}\boldsymbol{\epsilon}_1 \right] \\ &= -\frac{1}{2} E_{p(\boldsymbol{\epsilon}_1)} [\log |\tilde{G}|^2] - \frac{1}{2} E_{p(\boldsymbol{\epsilon}_1)} [\boldsymbol{\epsilon}_1^\top \boldsymbol{\epsilon}_1] + \frac{1}{2} E_{p(\boldsymbol{\epsilon}_1)} [\boldsymbol{\epsilon}_1^\top \tilde{G}^\top \tilde{G}\boldsymbol{\epsilon}_1] \\ &= -\log |\tilde{G}| - \frac{1}{2} \cdot M + \frac{1}{2} \text{trace}(\bar{\Omega}^\top) \\ &= -\log |\tilde{G}| - \frac{1}{2} \cdot M + \frac{1}{2} \cdot M \\ &= -\log |\tilde{G}|, \end{aligned}$$

where $E_{p(\boldsymbol{\epsilon}_1)} [\boldsymbol{\epsilon}_1^\top \tilde{G}^\top \tilde{G}\boldsymbol{\epsilon}_1] = \text{trace}(\bar{\Omega}^\top)$ is a result based on equation (318) from Matrix Cookbook (Petersen et al., 2008).

Thus, the ELBO function for KVC can be expressed as:

$$\mathcal{L}(q) = \mathbb{E}_q [\log h(\boldsymbol{\theta})] - \sum_{j=1}^M \mathbb{E}_{q_j} [\log q_j(\boldsymbol{\theta}_j; \boldsymbol{\lambda}_j)] + \log |\tilde{G}|.$$

Such a result simplifies $\nabla_{\boldsymbol{\lambda}_{\text{vc}}} \mathcal{L}(\boldsymbol{\lambda})$ for KVC:

$$\nabla_{\boldsymbol{\lambda}_{\text{vc}}} \mathcal{L}(\boldsymbol{\lambda}) = \mathbb{E}_{f_\epsilon} \left\{ \left[\frac{d\boldsymbol{\theta}}{d\boldsymbol{\lambda}_{\text{vc}}} \right]^\top \nabla_{\boldsymbol{\theta}} \left(\log h(\boldsymbol{\theta}) - \sum_{j=1}^M \log q_j(\boldsymbol{\theta}_j; \boldsymbol{\lambda}_j) \right) \right\} + \nabla_{\boldsymbol{\lambda}_{\text{vc}}} \log |\tilde{G}|. \quad (\text{A5})$$

To conclude, we use (A4) and (A5) as the re-parameterized gradients for KVC-G.

Part D: Additional empirical information

Table A1: Computational time per 1000 steps (in proportion to GMF) for different VAs in the logistic regression

Dataset Name	Low-Dimensional Real				High-Dimensional Real				High-Dimensional Simulated		
	krkp	mushroom	spam	iono	cancer	qsar	simu1	simu2	simu3		
Dataset Size ($n \times m$)	3196x38	8124x96	4601x105	351x112	42x2001	8992x1024	5Kx10K	20Kx10K	100Kx10K		
<i>Benchmark VAs:</i>											
GMF	0.40	0.50	0.47	0.34	0.52	2.49	12.60	53.64	285.19		
GMF (AG)	0.85	0.90	0.90	0.81	0.88	0.92	0.98	0.99	0.99		
G-F5	1.97	1.97	2.08	2.35	40.53	4.22	56.81	14.41	3.32		
GC-F5	3.51	3.27	3.52	4.38	42.48	4.61	55.01	14.53	3.52		
G-20	2.00	2.03	2.25	2.69	40.48	3.56	58.05	14.51	3.53		
GC-20	3.52	3.39	3.65	4.76	43.41	4.03	59.43	14.76	3.52		
BLK	3.19	2.89	3.07	3.83	90.65	8.72	94.80	23.25	5.69		
BLK-C	4.49	4.26	4.53	5.82	93.60	9.48	94.63	23.47	5.70		
<i>Vector Copula Model VAs:</i>											
A1: (GVC-F5 & M1)	4.15	5.28	6.13	8.35	1494.00	69.51	CI	CI	CI		
A2: (GVC-F5 & M1+YJ)	5.72	6.73	7.82	10.33	1500.01	70.11	CI	CI	CI		
A3: (GVC-I & M1)	1.41	1.35	1.39	1.60	1.44	1.09	1.09	1.02	0.99		
A3 (AG): (GVC-I & M1)	1.14	1.12	1.14	1.24	1.17	0.90	1.02	1.00	1.00		
A4: (GVC-I & M1+YJ)	2.70	2.47	2.57	3.28	4.10	1.44	1.53	1.12	1.01		
A5: (GVC-I & M2)	3.39	3.22	3.50	4.44	96.75	9.52	102.14	26.72	6.29		
A6: (GVC-I & M2+YJ)	4.94	4.55	4.84	6.45	100.04	9.97	103.24	26.79	6.28		

Note: The computational time (seconds) for GMF is reported in the table. The time of other VAs is divided by that from GMF. All VAs are trained with double precision on the CPU of Apple M3 Max. The gradients to update variational parameters are evaluated by 1000 times (100 times for simulated datasets, and then scale to 1000). The gradients are computed by Pytorch automatically except for GMF (AG) and A3 (AG). "AG" represents analytical gradients and "CI" represents computationally infeasible.

Table A2: List of Example Applications and Dimension of Posterior

Example	Model Type	Prior Type	Posterior Dimension d
E.g.1 (low-dim datasets) <i>krkp, mushroom, spam, iono</i>	Sparse Logistic Regression	Horseshoe	77, 193, 211, 225
E.g.1 (High-dim datasets) <i>cancer, qsar</i>	Sparse Logistic Regression	Horseshoe	4003, 2049
E.g.1 (Simulated datasets) <i>simu1, simu2, simu3</i>	Sparse Logistic Regression	Horseshoe	20001, 20001, 20001
E.g. 2 $r = 5, 10, 20, 30, 49$	Regularized Correlation Matrix	Bayesian LASSO	21, 91, 381, 871, 2353
E.g. 3	UCSV for U.S. Inflation	Autoregressive	572
E.g. 4	Additive Robust P-Spline	Autoregressive	89

Part E: Nested vector copula density

E.1: Re-parameterization trick

When one or more multivariate marginals of a vector copula model are themselves vector copula models, then this defines a “nested” vector copula. For example, consider the case where $M = 3$ and the nested vector copula is constructed from two bivariate vector copulas labeled “a” and “b”. The first has density c_v^a with marginals of size $d_1^a = d_1 + d_2$, $d_2^a = d_3$, and the second has density c_v^b with marginals of size $d_1^b = d_1$, $d_2^b = d_2$. Then, the VA density when C_v^a nests C_v^b is

$$\begin{aligned} q_\lambda(\boldsymbol{\theta}) &= c_v^a(\tilde{\mathbf{u}}_{12}, \tilde{\mathbf{u}}_3; \boldsymbol{\lambda}_{\text{vc}}^a) q_{12}(\boldsymbol{\theta}_1, \boldsymbol{\theta}_2) q_3(\boldsymbol{\theta}_3) \\ &= \underbrace{c_v^a(\tilde{\mathbf{u}}_{12}, \tilde{\mathbf{u}}_3; \boldsymbol{\lambda}_{\text{vc}}^a) c_v^b(\mathbf{u}_1, \mathbf{u}_2; \boldsymbol{\lambda}_{\text{vc}}^b)}_{\equiv c_v(\mathbf{u}_1, \mathbf{u}_2, \mathbf{u}_3; \boldsymbol{\lambda}_{\text{vc}})} \prod_{j=1}^3 q_j(\boldsymbol{\theta}_j) \end{aligned}$$

where $\mathbf{u}_j \in [0, 1]^{d_j}$, $\tilde{\mathbf{u}}_{12} \in [0, 1]^{d_1^a}$ and $\mathbf{u}_3 = \tilde{\mathbf{u}}_3 \in [0, 1]^{d_3}$. Here, c_v is the resulting nested vector copula, $\boldsymbol{\lambda}_{\text{vc}} = (\boldsymbol{\lambda}_{\text{vc}}^{a\top}, \boldsymbol{\lambda}_{\text{vc}}^{b\top})^\top$. This modular structure provides extensive flexibility, and is particularly useful as it facilitates the use of GVC-I and GVC-O (which are both limited to two blocks) in block dependent posteriors where $M > 2$. Specifically, we can choose C_v^a as a GVC or KVC and C_v^b as GVC-O, and use the following two-step re-parameterization trick to sample from a 3-block nested vector copula.

1. Sample $(\tilde{\mathbf{u}}_{12}, \tilde{\mathbf{u}}_3)$ from a two-block vector copula C_v^a .
2. Let $(\mathbf{u}_1^\top, \mathbf{u}_2^\top)^\top = \underline{\Phi} \{g_1(\underline{\Phi}^{-1}(\tilde{\mathbf{u}}_{12}), \boldsymbol{\lambda}_{\text{vc}}^b)\}$, where g_1 is the re-parameterization trick to sample from GVC-O.

We next prove that $c_v(\mathbf{u}_1, \mathbf{u}_2, \mathbf{u}_3; \boldsymbol{\lambda}_{\text{vc}})$ is a well-defined vector copula density. By definition, a vector copula density is a probability density $c(\mathbf{u}_1, \dots, \mathbf{u}_M)$ defined on uniform blocks such that each variable within \mathbf{u}_j is distributed independently as a uniform distribution ($j = 1, \dots, M$).

Proof. Partition $\tilde{\mathbf{u}}_{12}$ into $\tilde{\mathbf{u}}_1$ and $\tilde{\mathbf{u}}_2$ such that $\tilde{\mathbf{u}}_{12} = (\tilde{\mathbf{u}}_1^\top, \tilde{\mathbf{u}}_2^\top)^\top$, where $\tilde{\mathbf{u}}_1 \in [0, 1]^{d_1}$ and $\tilde{\mathbf{u}}_2 \in [0, 1]^{d_2}$. The two step re-parameterization trick can be represented as:

$$\begin{pmatrix} \mathbf{u}_1 \\ \mathbf{u}_2 \\ \mathbf{u}_3 \end{pmatrix} = \underline{\Phi} \begin{pmatrix} I_{d_1} & \mathbf{0}_{d_1 \times d_2} & \mathbf{0}_{d_1 \times d_3} \\ Q_2 \Lambda Q_1^\top & Q_2 \sqrt{I_{\tilde{d}} - \Lambda^2} & \mathbf{0}_{d_2 \times d_3} \\ \mathbf{0}_{d_3 \times d_1} & \mathbf{0}_{d_3 \times d_2} & I_{d_3} \end{pmatrix} \underline{\Phi}^{-1} \begin{pmatrix} \tilde{\mathbf{u}}_1 \\ \tilde{\mathbf{u}}_2 \\ \tilde{\mathbf{u}}_3 \end{pmatrix}$$

It is straightforward to see that $\mathbf{u}_1 = \tilde{\mathbf{u}}_1$ and $\mathbf{u}_3 = \tilde{\mathbf{u}}_3$. Thus, the elements within \mathbf{u}_1 and \mathbf{u}_3 are mutually independent, and are distributed as uniform distributions.

Let $\tilde{\mathbf{z}}_1 = \underline{\Phi}^{-1}(\tilde{\mathbf{u}}_1)$ and $\tilde{\mathbf{z}}_2 = \underline{\Phi}^{-1}(\tilde{\mathbf{u}}_2)$. Then, we have $(\tilde{\mathbf{z}}_1^\top, \tilde{\mathbf{z}}_2^\top)^\top \sim \mathcal{N}(0, I_{d_1+d_2})$ and $\mathbf{u}_2 = \underline{\Phi} \{z_2\}$ with

$$\mathbf{z}_2 = Q_2 \Lambda Q_1^\top \tilde{\mathbf{z}}_1 + Q_2 \sqrt{I_{\tilde{d}} - \Lambda^2} \tilde{\mathbf{z}}_2 \sim \mathcal{N}(0, I_{d_2})$$

followed by the result from Section 3.1.2 in the paper. Thus, elements within \mathbf{u}_2 are distributed independently as uniform distributions. \square

E.2: Empirical results

We use the nested vector copula to link the global shrinkage parameter $\tilde{\xi}$ to $\boldsymbol{\alpha}$ and $\tilde{\boldsymbol{\delta}}$ in the logistic regression and correlation matrix. Specifically, we choose C_v^b as GVC-I for $\boldsymbol{\alpha}$ and $\tilde{\boldsymbol{\delta}}$, and we choose C_v^a as KVC. As a result, a 3-block nested vector copula is used for $\boldsymbol{\theta} = (\boldsymbol{\alpha}^\top, \tilde{\boldsymbol{\delta}}^\top, \boldsymbol{\xi})^\top$. We use the same marginal construction as A4, and we name this method as A7. The extended empirical results (the last row) are shown as follows.

Table A3: ELBO values for different VAs (rows) in the regularized logistic regression with nine datasets (columns)

Dataset	Low-Dimensional Real				High-dimensional Real			High-Dimensional Simulated		
	krkp	mushroom	spam	iono	cancer	qsar	simu1	simu2	simu3	
Name										
Size ($n \times m$)	3196x38	8124x96	4601x105	351x112	42x2001	8992x1024	5Kx10K	20Kx10K	100Kx10K	
GMF	-382.01	-120.85	-856.77	-98.82	-77.59	-2245.10	-3641.64	-10844.22	-40735.67	
A4: (GVC-I & M1-YJ)	36.98	21.09	42.11	10.26	-0.27	87.93	185.63	753.43	1929.11	
A6: (GVC-I & M2-YJ)	18.85	20.05	40.80	10.55	-1.75	85.45	121.51	700.10	1857.95	
A7: (Nested & M1-YJ)	37.11	20.92	42.55	9.96	-0.31	87.66	188.73	753.66	1932.40	

Note: We keep the results from A4 and A6 in Table 2 because they are the optimal methods for this example. ELBO values are reported for GMF, and the differences from these values are reported for the other VAs. Higher values correspond to higher accuracy, and the bold value in each column indicates the highest ELBO value for the dataset.

Table A4: ELBO values for different VAs for the regularized correlation matrix Σ

Number of U.S. States	$r = 5$	$r = 10$	$r = 20$	$r = 30$	$r = 49$
Dimension of θ	21	91	381	871	2353
GMF	-553.93	-1039.24	-2038.91	-3152.38	-5548.02
A4: (GVC-I & M1-YJ)	10.91	35.48	71.07	109.90	181.98
A6: (GVC-I & M2-YJ)	10.64	34.96	70.96	110.06	181.25
A7: (Nested & M1-YJ)	10.93	35.34	71.17	109.95	182.03

Note: We keep the results from A4 and A6 in Table 3 because they are the optimal methods for this example. The posterior is for the $(r \times r)$ regularized correlation matrix Σ of the Gaussian copula model for U.S. wealth inequality panel data. The columns give results for $r = 5, 10, 20, 30$ and 49 U.S. states, and the VAs (rows) are described in Section 4.2. ELBO values are reported for GMF, and the differences from these values are reported for the other VAs. Higher values correspond to greater accuracy, with the largest value in each column in bold.

Table A5: Computational time per 1000 steps (in proportion to GMF) for different VAs in the logistic regression

Dataset Name	Low-Dimensional Real				High-Dimensional Real				High-Dimensional Simulated			
	krkp	mushroom	spam	iono	cancer	qsar	simu1	simu2	simu3	simu1	simu2	simu3
Dataset Size ($n \times m$)	3196x38	8124x96	4601x105	351x112	42x2001	8992x1024	5Kx10K	20Kx10K	100Kx10K	5Kx10K	20Kx10K	100Kx10K
GMF	0.40	0.50	0.47	0.34	0.52	2.49	12.60	53.64	285.19	12.60	53.64	285.19
A4: (GVC-I & M1+YJ)	2.70	2.47	2.57	3.28	4.10	1.44	1.53	1.12	1.01	1.53	1.12	1.01
A6: (GVC-I & M2+YJ)	4.94	4.55	4.84	6.45	100.04	9.97	103.24	26.79	6.28	103.24	26.79	6.28
A7: (Nested & M1+YJ)	4.18	3.74	3.83	4.99	5.54	1.75	1.66	1.17	1.01	1.66	1.17	1.01

Note: We keep the results from A4 and A6 in Table A1 because they are the optimal methods for this example. The computational time (seconds) for GMF is reported in the table. The time of other VAs is divided by that from GMF. All VAs are trained with double precision on the CPU of Apple M3 Max. The gradients to update variational parameters are evaluated by 1000 times (100 times for simulated datasets, and then scale to 1000). The gradients are computed by Pytorch automatically.